Small-Scale Biological and Physical Structure in a Tidally Mixed Fjord

by

Isabelle Gaboury

B.Sc., University of Victoria, 2000

A Thesis Submitted in Partial Fulfillment of the
Requirements for the Degree of

MASTER OF SCIENCE

in the School of Earth and Ocean Sciences

Supervisors: Drs. R. G. Lueck and C. J. R. Garrett

Abstract

While zooplankton patchiness has long been recognized as an important aspect of zooplankton ecology, the nature and role of such patches at scales smaller than one metre continue to be poorly understood. In June, 2001, a horizontally towed vehicle was used to simultaneously measure zooplankton acoustic backscatter and turbulent dissipation rates around the sill of Knight Inlet, British Columbia. By repeatedly insonifying volumes of water at a range of up to 20 m, it was possible to observe both the extent and the persistence of zooplankton patchiness. Micro-aggregations, approximately 10-30 cm in width, were observed throughout the region, with local widths and shapes reflecting the sizes and number densities of organisms present. Aggregations were found to be less stable at higher dissipation rates, particularly at depths dominated by smaller organisms, consistent with disruption by turbulent velocity fluctuations in excess of zooplankton swimming speeds.

Table of Contents

List of Tables

List of Figures

Acknowledgements

I have been fortunate to receive help from many people and in many forms during my time at UVic. My heartfelt thanks to everyone who helped me collect data, took the time to puzzle over problems with me, or simply provided words of encouragement along the way.

In particular, I would like to thank my committee, as well as Dr. Hide Yamazaki, who joined us for the first few meetings, for their advice and for the many stimulating discussions. The members of the Ocean Turbulence Laboratory, Rolf, Paul Macoun, Tetjana Ross, and Roland Gaboury, all put in considerable effort at all stages of the data collection process, and have been excellent company in the past few years. The professionalism and skill of the crew of the *CCGS Vector*, as well as the tireless enthusiasm of the Ocean Turbulence Lab and the Ocean Physics Group, made it possible to do more in a few days at sea than I would have dreamt possible. Thanks also to Dr. Angelica Peña, for the use of the fluorometer.

I am very grateful to ASL Environmental Sciences Ltd., who loaned us the WCP, and who have provided the technological expertise that made this project possible. In particular, my thanks to Murray Clarke, for the many hours he spent adapting the WCP to our purposes and helping me interpret the acoustic data.

Last, but certainly not least, I would like to thank those who have laboured behind the scenes to keep me focussed, without letting me lose my sense of humour. My husband, Roland, has been there for me in so many ways that I cannot even begin to list them, and I can only say thank you for everything. Thanks also to my family, as well as to Roland's, for their encouragement and support.

Chapter 1

Introduction

While the well-lit surface layers of the world's oceans support a tremendous biomass of planktonic organisms, these organisms in fact exist as a very dilute suspension of life in a very large, three-dimensional medium. Given the small sizes of planktonic animals, their limited perceptive ranges, and the large separations between them, encounters with mates or food particles might be expected to be relatively infrequent. Yet, the growth and reproductive rates observed in zooplankton populations indicate that individuals do in fact find both the resources, with considerably greater success than might be predicted from theoretical and laboratory work (e.g., Davis et al. 1991, Dower et al. 1997). How is this possible? The answer may lie in the fact that zooplankton and their prey are not, in fact, distributed homogeneously; either by choice or by chance, planktonic organisms are often closer to a neighbour than their average number densities would suggest.

In work started in the 1930s and continuing today, zooplankton have been observed to be patchy at scales from hundreds of kilometres to centimetres (Mackas et al. 1985, Denman and Dower 2001). At large scales, distributions reflect the paths of ocean currents and the mixing effects of winds and waves, as well as zooplankton life histories and programmed behaviours such as vertical migration (Mackas et al. 1985). Moving through successively smaller scales, biological processes play an increasing role in shaping distributions, until, at the smallest scales, we enter the world as perceived by individual zooplankters. At these scales, zooplankton can no longer be considered as passive particles; rather, their dealings with the environment and with each other are shaped by the way in which they sense and respond to various elements

of their immediate surroundings, including the proximity of prey, predators, and other members of the same species. One of the ways these forces and behaviours are expressed is in the small-scale distributions of zooplankton. Micro-scale patchiness, and the forces that influence it, remain poorly understood. However, the effect of these patterns on how organisms interact with food, predators, and mates makes this an important aspect of zooplankton ecology, particularly where distributions may be modulated by environmental variables.

Turbulence may significantly impact the extent and nature of patchiness in the plankton. While zooplankton can only sense large-scale advective motions via their effects on variables such as pressure and light intensity, turbulent velocity fluctuations occur on scales comparable to the body sizes and ranges of travel of individual organisms, and may be directly perceived. At high dissipation rates, these velocity fluctuations may be large enough to actively break apart patches and redistribute organisms. At lower levels, turbulence may affect organisms through a variety of processes related to feeding, sensory mechanisms, and interactions with other animals (Dower et al. 1997, Yamazaki et al. 2002), which may translate into changes in aggregative behaviours. As with strictly biological processes, the way in which turbulence affects micro-scale distributions will depend on the sizes, sensory abilities, and swimming speeds of the organisms involved, and perhaps on other environmental factors (e.g., food concentration).

The goal of the work described in the following chapters was to explore zooplankton distributions at sub-metre scales, using towed acoustics. Specifically, this research sought to address the following questions:

- How may towed, single-frequency acoustics be used to collect information on the horizontal distributions of zooplankton?
- How are zooplankton distributed at horizontal scales smaller than one metre? If structure exists, what are the relevant scales?
- How are distributions affected by biological and physical variables? In particular, how do the patterns observed vary with local species composition of the zooplankton and with changing levels of turbulence?

The data used to explore these questions were collected near the sill of Knight Inlet, British Columbia, in June of 2001. The zooplankton community in the Inlet

experiences regularly varying levels of turbulence, produced as tidal flows are funnelled over a shallow sill. Over the course of three days, two main tools were used to measure physical and biological variables during an entire tidal cycle. TOMI (the Towed Ocean Microstructure Instrument), a horizontally towed instrument supporting a suite of navigational and environmental sensors, was used to collect fine- and micro-scale temperature, salinity, fluorescence, and velocity shear data. The WCP (Water Column Profiler) was mounted on TOMI, and acoustically measured undisturbed zooplankton distributions at ranges up to 20 m. As TOMI was towed back and forth across the sill region, the WCP was used to repeatedly insonify volumes of water, yielding observations of horizontal zooplankton distributions with a resolution of a few centimetres, and also providing some estimate of the persistence of these patterns. Measurements from these two instruments were supplemented by data from echosounders and an ADCP mounted on the ship, which observed larger-scale flow patterns and zooplankton distributions. In addition, vertical net tows were conducted between TOMI/WCP tows, yielding information on the zooplankton community structure. Combining these data sets, it was possible to produce a picture of zooplankton distributions as they changed in response to varying turbulent intensities.

The next chapter summarizes some of the research that has been done on zooplankton patchiness, and sets the theoretical background for the use of acoustic methods in measuring zooplankton distributions. Chapter 3 describes the instrumentation used in Knight Inlet, the survey area itself, and the data that were collected. Chapter 4 describes the flow over the sill of Knight Inlet, the zooplankton community in the area, and our observations of zooplankton distributions over the course of the tidal cycle. These findings are discussed in light of existing research in Chapter 5, and are summarized in Chapter 6, along with some ideas for future work.

Chapter 2

Background and Theory

For almost three-quarters of a century, it has been recognized that plankton are distributed non-homogeneously in marine environments, despite the absence of obvious physical barriers to transport (Mackas et al. 1985, Denman and Dower 2001). In fact, zooplankton distributions are patchy on a wide range of spatial and temporal scales, as a result of a variety of physical and biological processes. The gradual exploration of these levels of heterogeneity over the decades has been closely tied to technological developments, which have allowed plankton distributions and other oceanographic properties to be sampled at finer and finer resolutions. The following section will provide an overview of some of the methodologies and observations that have shaped our current understanding of zooplankton patchiness and the forces that drive it. In Section 2.2, acoustics will be introduced as one of the major tools used to measure zooplankton distributions, and some of the theory and practice of zooplankton acoustics will be discussed, particularly as applied to our survey in Knight Inlet.

2.1 Small-Scale Zooplankton Distributions

2.1.1 Patchiness in Zooplankton Distributions

Because of the importance of discrete zooplankton sampling methods (e.g., nets), heterogeneity in zooplankton distributions was identified relatively early in the history of modern biological oceanography, if nothing else as a statistical nuisance affecting sampling design (Mackas et al. 1985). As this variability was studied in greater detail, initially on scales of tens and hundreds of kilometres, distributions were found to be

structured; not only did clumps or patches exist on a range of scales, but these patterns were correlated with other oceanographic variables (Denman and Platt 1978, Mackas and Boyd 1979). As sampling resolutions improved and more simultaneous measurements were made of zooplankton abundance and water properties, examples of patchiness were observed on scales of metres vertically and hundreds of metres horizontally, and in some cases were found to be associated with particular physical features, such as water masses, topography, and distributions of velocity shear (e.g., Mackas et al. 1993, Gallager et al. 1996, Mackas et al. 1997, Ashjian et al. 2001). As patterns were observed on scales relevant to zooplankton behaviour, explanations of zooplankton distributions also began to incorporate a significant biological component (e.g., Mackas et al. 1997). Additionally, theoretical and field work pointed to the importance of patchiness to zooplankton survival, growth, and reproduction (e.g., Davis et al. 1991, Tiselius 1992). More recently still, it has become possible to observe zooplankton distributions and behaviour at scales smaller than a metre, so that interactions and patterns at the scale of individual organisms may be considered. Vertically, layers as thin as 5 cm have been observed, and associated with swimming behaviour in response to physical characteristics of the water column (Gallager et al. 2004). Horizontally, examples exist of patches on scales of metres and tens of metres (Gallager et al. 1996, Currie et al. 1998), and micro-aggregations as small as 20 cm have been observed (Davis et al. 1992). Meanwhile, other studies have suggested that micro-scale patchiness may not always exist (De Robertis 2002), emphasizing the need to understand the processes that influence zooplankton distributions, and the scales at which they act.

The discovery of zooplankton patchiness at increasingly small scales has been tied to advances in the technology used to sample zooplankton distributions. Early work depended on zooplankton sampling with nets and pumps, for which the resolution is limited not only by the dimensions of the instrument itself, but also by the need to manually sort and count zooplankton in each sample collected. The use of methods which continuously collect zooplankton data electronically, and often remotely, made it possible to consider patterns as small as the resolution of the instrument; one such tool is acoustics, which has seen considerable development over the decades (Holliday et al. 2003). In the last ten years or so, these tools have been refined to the point where it is possible to measure sub-metre scale patchiness, simultaneously with relevant physical and biological variables; examples of such equipment include

Horizontal length scale	*Time scale*	*Processes*
$\gtrsim$ 100 km	months	hydrography, large-scale flows, primary productivity patterns, life history
kms to 10s of kms	days to weeks	advection, upwelling, accumulation (e.g., fronts), population growth (e.g., blooms), episodic predation stress, migratory behaviour
10s to 100s of metres	hours to days	large turbulent eddies, internal waves, formation of swarms, vertical migration
metres	minutes to days	large turbulent eddies, internal waves, vertical migrations, formation of small aggregates and swarms, algae-herbivore interactions
mms to cms	seconds to ?	microscale turbulence, food concentration, formation of mating clusters, individual-scale behaviours

Table 2.1: Range of temporal and spatial scales relevant to zooplankton patchiness, and examples of physical and biological processes acting at each (Mackas et al. 1985, Denman and Gargett 1995, Pinel-Alloul 1995, Folt and Burns 1999).

optical plankton counters (e.g., Currie et al. 1998), cameras (e.g., the VPR (Davis et al. 1992)), and sophisticated acoustics (e.g., OASIS (Jaffe et al. 1998)). However, although these methods have shown considerable success in observing zooplankton distributions and behaviour, work is still ongoing; measurements of zooplankton abundance at scales smaller than one metre are still few, and many questions remain unanswered, particularly at scales of a few centimetres.

Many of the issues that remain to be addressed concern the physical and biological causes of zooplankton micro-patchiness. Driving forces are better understood at large scales, for which distributions can be explained largely by physical processes, treating zooplankton basically as passive particles (Table 2.1); zooplankton distributions may be directly shaped by advection and mixing, or be influenced indirectly, for example by factors influencing phytoplankton growth (e.g., upwelling). At scales of tens and hundreds of metres, water motions and properties may interact with large-scale swimming behaviour such as vertical migrations, allowing some zooplankton to exert a level of control over their horizontal and vertical distributions (e.g., Mackas et al. 1993, 1997). Some water motions are involved at centimetre scales as well, mainly turbulence. However, turbulence alone is not enough to explain micro-scale patchi-

ness (Yamazaki and Squires 1996, Gallager et al. 2004), and most patterns at these scales must be explained in terms of random or directed swimming by zooplankton. Because of the difficulty in observing such behaviour in the field, and in establishing the reasons behind them, the biological mechanisms of micro-scale patch formation remind poorly understood. However, a number of processes may be involved:

- Feeding: Zooplankton can respond to increased food concentrations by changing their swimming patterns, allowing them to remain within food patches (Davis et al. 1991, De Robertis 2002). However, as zooplankton have been shown to be patchy at smaller scales than phytoplankton (Denman and Dower 2001), this cannot account for the smallest zooplankton patches. The formation of social aggregations may also increase the efficiency of feeding currents (Ritz 2000), perhaps motivating the active formation of such groups.

- Mating: Zooplankton find mates by complex cues and behaviours, and may interact for some time in the process (Strickler 1998, Yen et al. 1998, Yamazaki et al. 2002). Given the relative scarcity of mates at average zooplankton densities, the formation of mating aggregations may be important to zooplankton life cycles (Folt and Burns 1999). This mechanism was believed to be the cause for the smallest patches described in the literature, the small (approximately 20 cm) monospecific aggregations observed by Davis et al. (1992).

- Predator avoidance: Aggregation may serve to protect organisms from predation to some extent, e.g. through group avoidance strategies (Ritz 2000).

- Energy expenditure: Organisms swimming within a cohesive group may be able to take advantage of the wakes shed by their neighbours to reduce their sinking rates; this may in turn allow aggregated zooplankton to reduce their metabolic costs (Ritz 2000).

Given the importance of each of these processes, patchiness and the way in which it is used by organisms have the potential to significantly impact the growth and reproductive success of individual organisms, which will in turn be reflected by overall population size. In addition, physical processes may play a role; in particular, turbulence has been shown to affect individual zooplankters in a variety of ways (Dower et al. 1997, Yamazaki et al. 2002). As this is particularly relevant to our survey in

Knight Inlet, the effects of small-scale turbulent motions on zooplankton distributions are discussed in the next section.

2.1.2 Effects of Small-Scale Turbulence

Unlike larger-scale flow patterns, turbulent motions occur on temporal and spatial scales that are similar to those on which zooplankton interact with their environment (body sizes, perceptive ranges, distances of swimming "hops"). At these scales, turbulence is random, three-dimensional, intermittent, and isotropic (Gargett 1997, Yamazaki et al. 2002), and so represents a chaotic motion, unlike properties such as light and temperature, which zooplankton can follow along a gradient. In addition, the flows are complex, and any temporary flow structures that occur (e.g., Abraham 1998, Yamazaki et al. 2002) may be perceived and responded to by zooplankton.

The range of scales over which turbulent eddies exist is bounded at the upper end by vertical stratification, and at the lower end by molecular viscosity. The largest and smallest eddies allowed by these forces are described by the Ozmidov and Kolmogorov length scales, respectively:

$$L_O = \sqrt{\epsilon/N^3} \tag{2.1}$$

$$L_K = (\nu^3/\epsilon)^{1/4}, \tag{2.2}$$

where N is the buoyancy frequency, $\nu \approx 10^{-6}\,\mathrm{m^2 s^{-1}}$ is the kinematic viscosity, and ϵ is the dissipation rate, proportional to the variance of the shear (Lueck et al. 2002). For conditions such as those observed in Knight Inlet, turbulent eddies range in diameter from centimetres or metres for the largest overturns, to millimetres for the smallest eddies. A characteristic velocity at a given length scale may be obtained by summing the velocity fluctuations due to eddies up to the scale of interest, and is related to both the length scale and the dissipation rate,

$$U \approx (\epsilon L)^{1/3}. \tag{2.3}$$

(Note that this equation leaves out a constant of proportionality of order one.) Applying Eqn. 2.3 to the length scales described by Eqns. 2.1-2.2, typical velocity fluctuations are found to be on the order of a few centimetres per second at the Ozmidov length scale, and a few millimetres per second at the Kolmogorov length scale. The

way in which individual organisms and groups experience such eddies depends on their sizes. Eddies larger than a cluster produce strain along some axis of the patch, potentially changing its shape or pulling it apart. At smaller scales, eddies are experienced as chaotic local velocity fluctuations, and the resulting shear may homogenize patches. In addition, the smallest eddies may occur on scales similar to the body sizes and sensory ranges of zooplankton, and will influence how an individual zooplankter perceives and interacts with its immediate environment. Note that while Eqn. 2.3 provides a measure of the scales of velocity fluctuations an organism may encounter, the actual velocities "felt" by a single organism will be intermittent, with higher dissipation rates being experienced as more frequent, stronger fluctuations.

Turbulence may influence the growth and reproductive success of zooplankton in a variety of ways; good reviews on this topic include those by Mackas et al. (1985), Dower et al. (1997), and Yamazaki et al. (2002). In particular, the following processes illustrate some of the ways in which turbulence may influence zooplankton distributions:

- *Patch disruption:* Zooplankton will only be able to maintain aggregations if their swimming speeds are greater than the relative velocities experienced over the aggregation, i.e. if its members are not being pulled apart faster than they can swim toward one another (Yamazaki and Squires 1996). Even when it is possible to form patches, it may not be worthwhile for zooplankton to do so if the energetic costs of swimming outweigh the benefits of aggregating.

- *Feeding and predation:* Turbulence may disrupt phytoplankton patches, as well as change the rates of encounter between predators and prey (Davis et al. 1991, Dower et al. 1997). Such processes may require that zooplankton change their foraging techniques to maximize food intake, and/or modify their behaviour to avoid being consumed (e.g., Costello et al. 1990, Kiørboe et al. 1996, Dower et al. 1998). Such modifications in behaviour will be reflected in spatial distributions.

- *Mating:* Turbulent mixing may dilute and disrupt the chemical trails involved in mate tracking by some zooplankton species (Yen et al. 1998). However, it has been proposed that the existence of organized flow structures in turbulent fields may also play a role in the location of mates (Yamazaki et al. 2002), such that not all levels of turbulence are necessarily disruptive.

- *Communication:* While it is not known how zooplankton communicate to maintain patches, it seems likely that non-visual cues, e.g. chemical or hydrodynamic signals, are involved (Haury and Yamazaki 1995, Ritz 2000). These may be disrupted by turbulent motions, making patch maintenance difficult or impossible.

For a particular species, location, and set of conditions, the net effect of turbulence on zooplankton distributions will depend on the characteristics of the organisms involved, as well as their reasons for aggregating. While it is certain that zooplankton swimming speeds will be inadequate to maintain aggregations at some turbulent velocities, it is not clear what is likely to happen at low to intermediate velocities, or in the slower cores of large eddies. Because of the complexity of these processes, and the sampling challenges associated with measuring them, the effect of turbulence on zooplankton distributions remains poorly understood.

2.2 Acoustic Measurements of Zooplankton Distributions

Sound has been used to measure zooplankton distributions since the 1940s, when sound scattering layers were first identified and associated with zooplankton (Holliday 1980). Since then, refinements in echosounder technology have made it possible to observe zooplankton at multiple frequencies and at increasingly high resolutions (Holliday et al. 2003). Simultaneously, models have been developed to associate backscattering intensity with the physical characteristics of the objects being insonified, making it possible to interpret acoustic data and use them as a tool to measure zooplankton biomass, distributions, and properties (e.g., Stanton et al. 1994, Benfield et al. 1998, Chu et al. 2000, Holliday et al. 2003). In the following sections, the theory of zooplankton backscattering will be introduced, along with some of the models that have been developed to describe backscatter from organisms such as those found in Knight Inlet. In addition, some of the complications that may arise when attempting to interpret real acoustic data will be discussed.

2.2.1 Backscattering of Sound by Zooplankton

Basic Physics

In its simplest form, scattering from zooplankton may be described in terms of an idealized small body, which is small enough and far enough from the transducer that the spherical acoustic waves that are transmitted and reflected may be approximated as plane waves. Here we will also assume that the transducer is a combined transmitter/receiver, so that the transducer measures only sound that is reflected back along the incident ray path, i.e. backscattered sound.

The wave that is incident upon the scatterer has travelled a distance R from the transducer, resulting in losses in amplitude due to spherical divergence and energy absorption and scattering by the medium, such that the peak pressure of the incident wave is

$$P_{inc} = P_0 10^{-\alpha R/20} R^{-1}, \tag{2.4}$$

where P_0 is the peak pressure of the wave as it leaves the transducer and α describes the absorption of sound by seawater (in dB/m) (Medwin and Clay 1998). When the incident wave reaches the object, a portion of it diffracts around and past the object, while another part of it is reflected as another wave, which propagates outward and back toward the transducer. The intensity of the backscattered signal received by the transducer may be related to the incident pressure by the backscattering cross-section, σ_{bs}, of the scatterer:

$$P_{scat} = P_{inc}\sqrt{\sigma_{bs}}(10^{-\alpha R/20} R^{-1}) = P_0\sqrt{\sigma_{bs}}(10^{-2\alpha R/20} R^{-2}). \tag{2.5}$$

Note that while the backscattering cross-section is expressed as an area (i.e., units of m^2), it does not necessarily correspond to any dimension of the object. The ability of the scatterer to reflect sound is affected not only by its size and shape, but also by its material properties, specifically its density and sound speed.

The backscattering cross-section is often expressed as a logarithm, referred to as the target strength:

$$TS = 10\log\left(\frac{\sigma_{bs}}{1\,\mathrm{m}^2}\right), \tag{2.6}$$

In zooplankton acoustics, the transducer usually receives scattered waves from many such objects simultaneously, and it is appropriate to consider the logarithmic backscat-

tering cross-section per unit volume, referred to as the scattering volume:

$$Sv = 10\log\left(\frac{\sigma_{bs}}{U}\right) = TS - 10\log_{10}(U), \tag{2.7}$$

where U is the volume (in cubic metres) insonified by the transducer (see Section 3.1.3).

The way in which sound interacts with the object depends on the size of the object relative to the wavelength of sound used to insonify it. This gives rise to the discussion of scattering regimes (Fig. 2.1), which may be defined in terms of ka, where $k = 2\pi f/c$ is the acoustic wavenumber and a is the size of the scatterer:

1. Rayleigh scatter ($ka \ll 1$): For small objects and/or long wavelengths, much of the incident wavefront diffracts around the body, and the portion of the energy that is scattered may be approximated as a simple diverging, spherical wave, with intensity determined by the size, density, and compressibility of the organism. Backscattered intensity increases rapidly as a function of ka in this region (Fig. 2.1); for a sphere, the relative backscatter ($\sigma_{bs}/(\pi a^2)$) is proportional to $(ka)^4$ (Medwin and Clay 1998). One consequence of this for zooplankton acoustics is that very small organisms may be missed entirely if they scatter below the detection threshold of the transducer.

2. Geometric scatter ($ka \gg 1$): With short wavelengths and/or large objects, sound is reflected from surface elements as from a mirror ("specular" backscatter), and the intensity of the backscattered wave depends on the surface area of the object and interferences between the wavelets reflected from the various surface elements. Overall, σ_{bs} in this region increases as the cross-sectional area of the organism. However, because of interference effects between the various reflected and diffracted waves, it does so through a series of peaks and nulls (Fig. 2.1).

3. Transitional regime ($ka \approx 1$): Most often, zooplankton acousticians work near the boundary between the Rayleigh and geometric scattering domains. For such frequencies, sound mostly reflects from, rather than diffracts around, the small zooplankton; in addition, the frequencies are still low enough to minimize acoustic attenuation, which can limit the useful range of an echosounder system.

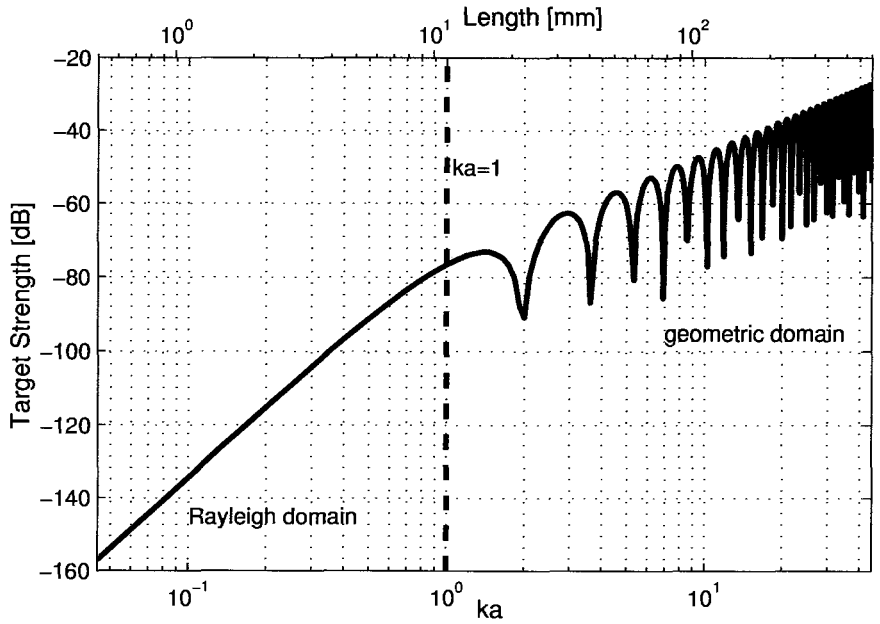

Figure 2.1: Target strength as a function of ka (wavenumber $\times$ organism radius) for a fluid cylinder of finite length (Eqn. 2.8, Stanton et al. 1993b), with dimensions and properties similar to a euphausiid. For reference, the corresponding body length of the organism is shown for a frequency of 307 kHz ($k = 1335\,\mathrm{m}^{-1}$).

> However, because both diffraction and reflection may play a role in this region, a general description of backscatter near $ka = 1$ is considerably more difficult than in the geometric or Rayleigh domains.

While a full description of the backscatter from zooplankton at the frequencies typically used to observe them is very complicated, the application of a series of assumptions and simplifications makes it possible to produce models that can be handled analytically and/or numerically.

Backscatter from a Single Organism

As even a simple mathematical description of the backscatter from a real object quickly becomes unwieldy, models are needed which preserve the essential features of such a description, but which are simple enough to be applied numerically. The earliest models of zooplankton backscatter approximated the organism as a homogeneous sphere (Anderson 1950); although these models were refined over the years, and

worked reasonably well in some cases, they were not adequate to describe the elongated shapes more typical of many zooplankton. These shapes were better described as straight or bent cylinders. Stanton (1988, 1989b) adapted the modal description of backscatter from an infinitely long cylinder to describe scattering from cylinders of finite length, producing a model which agreed well with exact solutions. However, the model was unwieldy, and involved a set of fairly limiting assumptions. Ray-based solutions proved more manageable for organisms with body properties not too dissimilar to sea water, and were particularly useful in describing the average backscatter from objects over a range of orientations (Stanton et al. 1993b, 1994). Nonetheless, they still depended on approximating complex shapes and properties as rather simple ones (spheroids and cylinders). More recently, models based on a modal description of backscatter have evolved in the case of fluid-like organisms to produce the Distorted Wave Born Approximation (DWBA) model, which can deal with more complicated shapes and physical properties, producing highly accurate estimates of zooplankton backscatter (Stanton et al. 1998, Stanton and Chu 2000). Nonetheless, simpler ray-based models such as those described by Stanton et al. (1994) remain in use, valued for their simplicity of application.

Models describing backscatter from fluid cylinders, i.e. cylinders with sound speed and compressibility similar to sea-water, are particularly relevant to the Knight Inlet survey, in that they may be applied to the crustaceans (copepods, amphipods, euphausiids) that dominated the zooplankton in the Inlet. The nature of the backscatter from such an object may be illustrated by considering the model developed by Stanton et al. (1993b) for a single fluid-like straight cylinder of finite length, involving a ray-based description of sound scattering from the object:

$$\sigma_{bs} = \left| \frac{-i}{2\sqrt{\pi}} e^{i\pi/4} e^{-i2ka\cos\theta} L\sqrt{ka\cos\theta} RDI \right|^2, \qquad (ka \gtrsim 0.1) \tag{2.8}$$

where the variables are defined in Table 2.2. This model describes geometric scatter from a cylinder, assuming that backscatter is dominated by reflections from the front and back interfaces of the organism. The terms describe reflection and transmission at each of these interfaces, and the changes in intensity and phase associated with these interactions, and also include corrections associated with effects caused by the ends of a finite-length organism. While the model is based on a description of scatter in the geometric regime, Stanton et al. (1993b) were able to extend its usefulness well

Variable	*Definition*
a	radius of cylinder cross-section
c	speed of sound in seawater
D	directivity pattern of scattering amplitude for an organism $D \approx \sin(kL\sin\theta)/(kL\sin\theta)$
f	frequency
g	ratio of mass density, organism vs. seawater
h	ratio of sound speed, organism vs. seawater
I	term describing interference between echoes from the front and back interfaces of a cylinder $I = 1 - T_{12}T_{21}e^{i4ka\cos\theta}e^{i\mu}$
k	acoustic wavenumber $k = 2\pi f/c$
L	organism length
L_{ebc}	effective length of a bent cylinder
R	reflection coefficient $R = (gh-1)/(gh+1)$
s_L	standard deviation of organism lengths
T_{12}, T_{21}	transmission coefficient, entering and leaving the organism, respectively $T_{12} = 2gh/(1+gh)$ $T_{21} = 2(gh)^{-1}/(1+(gh)^{-1}) = 2/(gh+1)$
β	twice the aspect ratio of an organism $\beta = L/a$
μ	phase advance (required to deal with finite cylinders with $ka \lesssim 1$) $\mu \simeq (-\pi/2)ka/(ka+0.4)$
σ_{bs}	back-scattering cross-section
θ	organism orientation ($\theta = 0°$ for broadside incidence)

Table 2.2: Variables used in the models for backscattering from finite-length, fluid-like cylinders (Stanton et al. 1993b,a, 1994). Variables are listed in alphabetical order.

into the Rayleigh domain.

Eqn. 2.8 may be adapted to a bent cylinder, by replacing the length L by an effective length, L_{ebc}, which takes into account the degree of bend (see Stanton et al. (1993b) for details):

$$(\sigma_{bs,bent})_{\theta=0°} = (\sigma_{bs,straight})_{\theta=0°}\left(\frac{L_{ebc}}{L}\right)^2. \tag{2.9}$$

Note that this effective length only makes sense if the cylinder is at broadside incidence and is uniformly bent away from the transducer (e.g., insonified from the top for

a euphausiid), making this formulation more restrictive than the straight-cylinder case. Although the correction to the length may be significant in some cases, L_{ebc} approaches L for deflections which are small compared to the wavelength, which is the case for the Knight Inlet work.

The description in Eqn. 2.8 is valid if the following assumptions are met: (1) the cylinder is surrounded by a fluid (seawater); (2) $ka \gtrsim 0.1$ (i.e., not too far into the Rayleigh regime); (3) $g, h \simeq 1$, (i.e., only dealing with weak scatterers); and (4) scattering is weak enough that effects such as multiple internal reflections can be ignored. These criterion were met for the crustacean and gelatinous zooplankton observed in Knight Inlet with the 307 kHz transducer. However, ka was too small to apply this model to the data collected with the 100 kHz ship-mounted echosounder.

Fig. 2.2 illustrates the dependence of backscattering cross-section on organism size and orientation as described by this model, for the sizes of organisms found in Knight Inlet. When considering single organisms, it is clear that target strength does not always increase with increasing organism size. Larger amphipods and euphausiids fall into the transitional scattering domain, and may scatter more weakly than smaller organisms. In addition, the observed target strength depends on the orientation of the organism. In order to deal with some of these sources of variability, it is useful to adapt the single-organism formulation described in this section to calculate the average return that might be expected from an organism whose length is not precisely known and whose orientation may vary; the result will be a "typical" backscattering cross-section, which may be compared with observed backscatter.

Average Backscatter

In order to calculate the backscatter from a group of similar organisms, it is necessary to describe the average backscatter from organisms with variable sizes and orientations. Individual contributions to the total scattering volume may then simply be summed:

$$Sv_{tot} = 10 \log_{10}(N\langle\sigma_{bs}\rangle/U), \tag{2.10}$$

where N is the number of organisms in the volume U (note that it is assumed here that N is small enough with respect to U that self-shading is not an issue). The average backscattering cross-section, $\langle\sigma_{bs}\rangle$, may be calculated based on the probability distributions of sizes and orientations of the organisms involved. For example, a

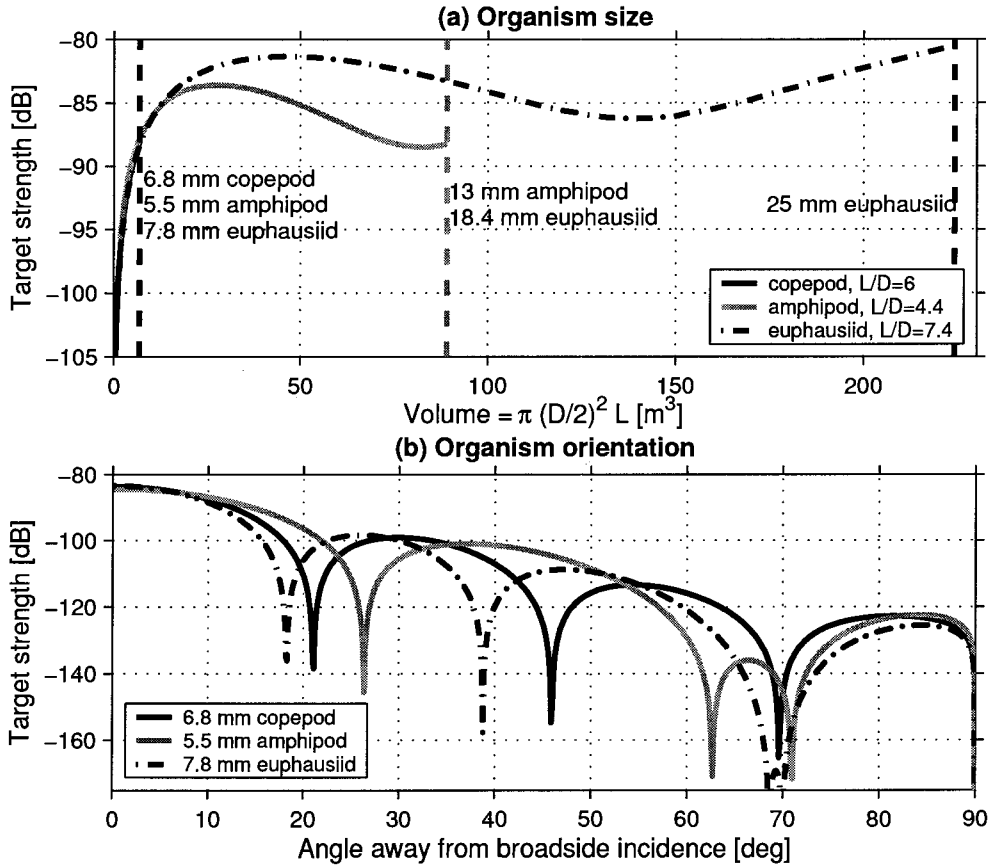

Figure 2.2: Target strength as a function of length and orientation for a randomly oriented, straight fluid cylinder (Eqn. 2.8, Stanton et al. 1993b). Sizes and length/width ratios are based on net data from Knight Inlet; vertical dashed lines in (a) mark the largest organism captured for each taxonomic group. Note that target strengths in (a) are for broadside incidence.

reasonable set of assumptions is that organisms are randomly oriented, and have a Gaussian distribution of lengths. Given the backscatter at broadside incidence for an organism of average size, $(\sigma_{bs})_0$, the average backscatter over such distributions can be calculated as follows:

$$\langle \sigma_{bs} \rangle_{\theta,L} = \iint W(\theta)\, W(L)\, D^2(\theta)\, (\sigma_{bs})_0\, dL\, d\theta, \tag{2.11}$$

where $W(\theta)$ and $W(L)$ are the probabilities associated with given angles of orientation and lengths, and $D(\theta)$ is the directivity pattern of backscattering amplitude, which

must be determined experimentally (Stanton et al. 1993a). For a uniform distribution of orientations and a Gaussian distribution of lengths,

$$W(\theta) = \frac{1}{2\pi} \quad \text{and} \quad W(L) = (\sqrt{2\pi}s_L)^{-1} e^{-(L-\overline{L})^2/(2s_L^2)}, \tag{2.12}$$

so that

$$\langle \sigma_{bs} \rangle_{\theta,L} = AR(\overline{L})^2 \langle |I_0|^2 \rangle_L \beta^{-1}) \tag{2.13}$$

where A is a combination of numerically determined coefficients, and $\langle |I_0|^2 \rangle_L$ is obtained by averaging I over the appropriate distribution of organism lengths. For a randomly oriented bent fluid cylinder, Stanton et al. (1993a) found $A = 0.08$, yielding the following compact form for the average backscatter, from Eqns. 2.9-2.13:

$$\langle \sigma_{bs} \rangle = 0.08 R^2 L^2 2\beta^{-1} \left\{ 1 - e^{-32\pi^2 f^2 a^2 s^2 c^{-2}} \cos\left[2\pi f a c^{-1} \left(4 - 0.5\pi (2\pi f a c^{-1} + 0.4)^{-1} \right) \right] \right\} \tag{2.14}$$

(Stanton et al. 1993a, 1994). This formula has been tested on crustacean scatterers, and found to agree well with measured backscatter (Wiebe et al. 1997). While it is based on bent cylinders, the correction due to the bend is not significant for the sizes of organisms and the frequency used in Knight Inlet; consequently, it may be used for all three dominant crustacean groups (copepods, amphipods, euphausiids) observed in the Inlet.

While most planktonic crustaceans can be approximated as fluid-like shapes, different models are required for organisms whose properties are dissimilar to those of seawater. Pteropods, in particular, have hard aragonite shells (g and h around 1.7 (Wiebe et al. 1997)), and are better modelled as an elastic-shelled sphere, with an average backscattering cross-section of

$$\langle \sigma_{bs} \rangle = \frac{100}{9} \pi^4 a^6 f^4 R^2 c^{-4} \left(1 + \frac{400}{9} \pi^4 f^4 a^4 c^{-4} \right)^{-1} \tag{2.15}$$

(Stanton 1989a, Stanton et al. 1994). This model still simplifies pteropod geometry considerably, and additional complications may arise from features such as the opening of the shell, for example; however, it is adequate for the calculation of average returns. Another group whose tissue properties contrast strongly with seawater are gas-filled siphonophores, for which backscatter is dominated by reflections from the small gas floats ($g \simeq 0.0012$, $h \simeq 0.22$ (Stanton et al. 1998)) which provide

flotation for the colony, as described by Stanton et al. (1994, 1996). However, the siphonophores in Knight Inlet were not gas-bearing, and hence can be described as fluid spheres (Stanton 1989a); furthermore, as the sound speed and density contrast of siphonophrore tissues are very low, the target strengths of these organisms will be much lower than those from crustaceans and pteropods (Stanton et al. 1994).

2.2.2 Backscatter from Sources Other than Zooplankton

Problems may arise when attempting to interpret acoustic data in terms of zooplankton returns when a portion of the backscatter actually comes from other sources. Examples of non-zooplankton sources of backscatter include the following:

- Electronic noise (see Section 3.1.3)
- Suspended sediments, particularly sand (Wiebe et al. 1997)
- Phytoplankton (mainly an issue at very high frequencies) (e.g., Selivanovsky et al. 1995)
- Fish (Holliday 1980)
- Bubbles (Medwin and Clay 1998)
- Turbulent microstructure (Ross 2003, Ross and Lueck 2003, 2004)

In most cases, the contributions from these sources are expected to be small. For example, most sedimentary particles and phytoplankton are very small, and so should fall well within the weakly scattering Rayleigh regime for most frequencies commonly used to observe zooplankton (Fig. 2.1). Except where breaking waves create large numbers of bubbles (e.g., in surf zones), these are not expected to be a significant source of backscatter. While fish are commonly co-located with zooplankton, and can scatter strongly, it is often possibly to separate these returns based on their intensity and distributions (e.g., Mackas et al. 1997, Trevorrow 2002).

Sound scattered from turbulent microstructure was the main source of non-zooplankton scatter in Knight Inlet, and is explored in depth by Ross (2003) and Ross and Lueck (2003, 2004), based on data collected during the 2001 survey. In areas with strong temperature and salinity stratification, such as Knight Inlet, turbulent stirring of these gradients at high dissipation rates may produce regions of

sharp contrast in sound speed, capable of scattering sound at levels comparable to zooplankton backscatter. While weak zooplankton scatterers will be invisible against this "background" of turbulent backscatter, and many more will be indistinguishable from it, Ross and Lueck (2004) offer an approach to separate zooplankton and turbulent backscatter in data such as those collected in this survey, where a given volume of water is insonified repeatedly with a horizontally oriented, towed echosounder. Because an organism is an object of finite size, it appears in the acoustic data as a discrete return with a specific horizontal dimension and location, both of which should be relatively constant from ping to ping, and with a scattering volume which depends on the organism's target strength and the portion of the total (range-dependent) insonified volume it occupies (Eqn. 2.7). In contrast, turbulence produces a volume backscattering effect; it appears as a background "noise" in acoustic images, rather than as a discrete object, and scatters at an intensity which is more or less independent of the volume being insonified (Ross and Lueck 2004). While this distinction is generally not enough to isolate zooplankton and turbulent backscatter in a way that would allow for accurate biomass estimates, it makes it possible to positively identify select targets as biological, allowing for at least limited observations of zooplankton distributions even in highly turbulent environments.

Chapter 3

Instrumentation and Methods

3.1 TOMI/WCP

The Towed Ocean Microstructure Instrument (TOMI) (Fig. 3.1) was developed by the Ocean Turbulence Laboratory for oceanic microstructure measurements, and was used as the data collection platform for this survey. It consists of a double-hulled main body, 4.5 m in length, stabilized by masts extending above and below the body, and by weights placed internally and on the bottom mast. The vehicle is slightly negatively buoyant in the water, and is dynamically lifted as it is towed horizontally by a neutrally buoyant Kevlar cable which also provides power and communications. A weighted section of cable approximately 50 m in front of the vehicle provides some decoupling from ship motion. The body contains two pressure cases, containing the signal conditioning and data telemetry electronics. A nose cone is attached to the forward pressure case, which extends about 0.3 m in front of the hull. This cone allows for attachment of thermistor and shear probes (Figs. 3.1(b), 3.2). The pressure case is padded in open-cell polyurethane foam, reducing contamination of the shear signal by vehicle vibrations.

The vehicle's position, orientation, and motion are measured by sensors on the ship and on the vehicle. DGPS position is recorded from the ship, and the vehicle's position may be approximated from the length of cable let out from the spool and the depth recorded by the Keller pressure transducer located at the back of the forward pressure case, near the midsection of the vehicle. Propeller-type flow-meters mounted on the upper and lower masts measure speed through the water. A compass in the

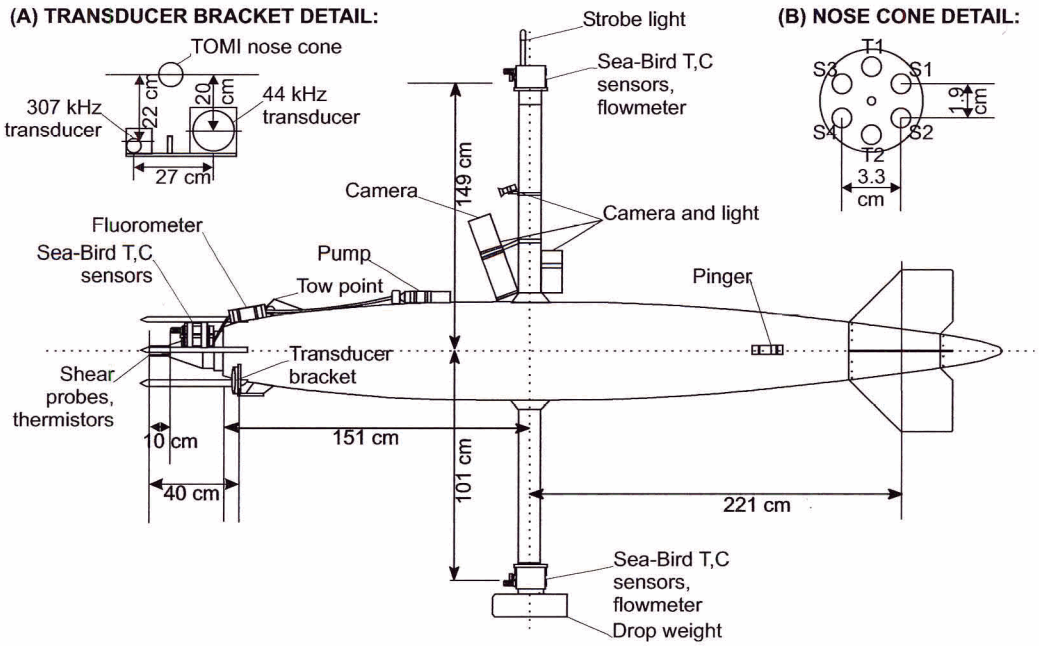

Figure 3.1: Schematic of the towed vehicle TOMI. Insets: (a) Transducer bracket. (b) Front view of the nose cone, with four shear probes and two thermistors. Modified from original figure by the Ocean Turbulence Lab.

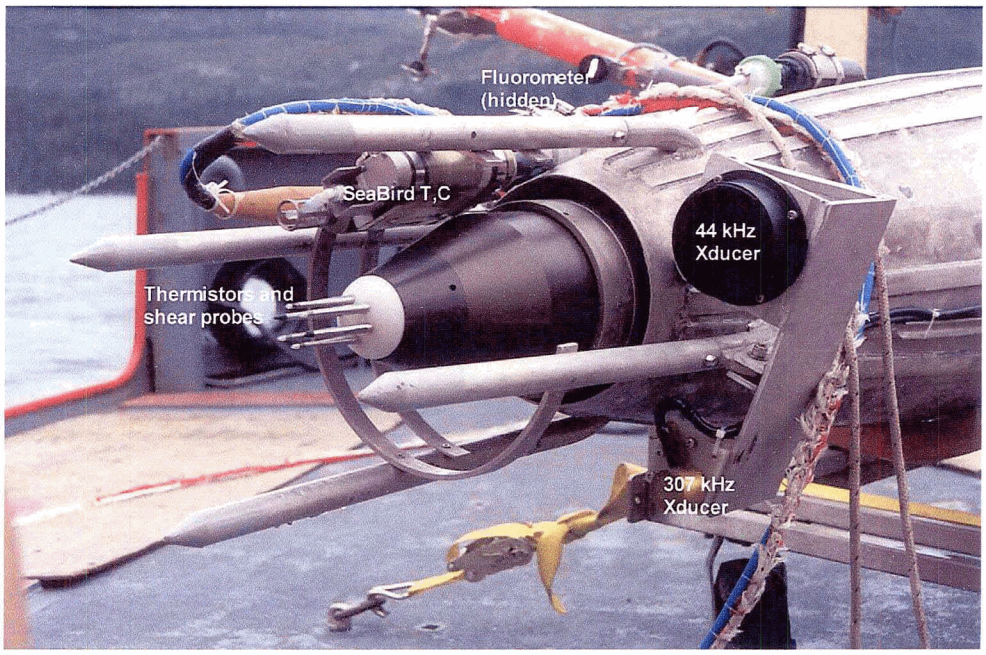

Figure 3.2: Nose of the Towed Ocean Microstructure Instrument, showing sensors and acoustic transducers.

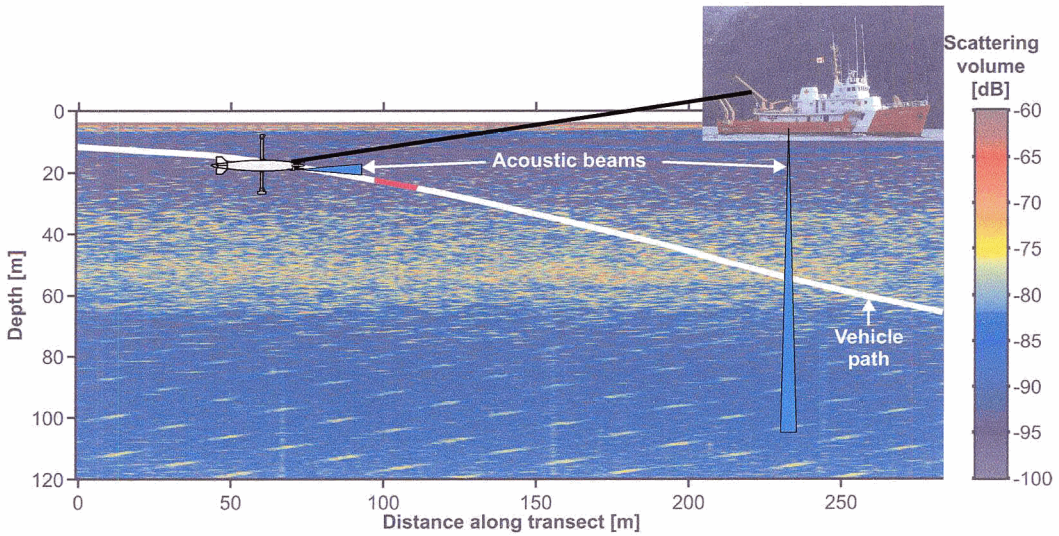

Figure 3.3: Acoustic sampling by the ship-mounted 100 kHz echosounder and the 307 kHz Water Column Profiler, showing TOMI towing arrangement and relative width of the acoustic beams. Ship and instrument not to scale. Highlighted section of the vehicle path is shown in detail in Fig. 3.4.

forward pressure case, along with three accelerometers and three angular rate sensors in the nose cone, add information on the orientation and motions of the vehicle.

Electronics in the front pressure case perform analog filtering/processing, sampling, and A/D conversion of data collected from TOMI's various sensors. The Ocean Data Acquisition System (ODAS) is used for communication between TOMI and the shipboard computers, which store and plot the data.

TOMI's sensors were complemented by the Water Column Profiler (WCP), developed by ASL Environmental Sciences Ltd. in Sidney, British Columbia. Two transducers mounted shortly aft of the nose cone measured acoustic backscatter in front of the vehicle, providing a much closer-range view of the zooplankton field than that afforded by ship-mounted echosounders (Fig. 3.3). Both 44 kHz and 307.2 kHz WCP's were installed; however, only the data from the higher-frequency system are discussed here.

Together, TOMI and the WCP simultaneously measured a suite of physical and biological variables, discussed below.

3.1.1 Fine-Scale Scalars: Temperature, Conductivity, and Fluorescence

Three sets of Sea-Bird temperature and conductivity sensors were mounted on TOMI: one on the nose of the vehicle, and one on each mast (to measure vertical gradients) (Figs. 3.1, 3.2). A WETLabs WETStar miniature fluorometer was mounted in-line with the pumped Sea-Bird sensors near the nose of the instrument, providing a record of chlorophyll fluorescence.

3.1.2 Temperature and Velocity Microstructure

Two Thermometrics FP07 thermistors and four airfoil shear probes mounted on the nose cone measured temperature and velocity mictrostructure (Fig. 3.2). In order to improve the resolution of the thermistor data, the signal was pre-emphasized by adding the signal to its derivative before digitization and recording, as described in Mudge and Lueck (1994). This was also done with the pressure signal (see Section 3.4.1).

The theory and application of shear probes is described elsewhere (Osborn and Crawford 1980, Lueck et al. 2002). To summarize, they consist of a piezoceramic beam oriented axially to the flow U, which flexes in response to one cross-component of the on-coming flow, producing a voltage proportional to the flow and to the travel speed:

$$E_p = 2\sqrt{2}SUw, \tag{3.1}$$

where E_p is the probe output voltage, S is the probe sensitivity (determined through calibration), U is the mean travel velocity of the vehicle through the water, and w is the cross-component of the flow (on this survey, all four probes were oriented to measure vertical velocity fluctuations). The voltage is differentiated before sampling,

$$E_s = G\frac{\partial E_p}{\partial t} = 2\sqrt{2}GSU\frac{\partial w}{\partial t}, \tag{3.2}$$

where E_s is the differentiated signal and G is the gain of the differentiator. Making use of the Taylor frozen field assumption, $\frac{\partial}{\partial t} = U\frac{\partial}{\partial x}$, the shear is thus proportional to the differentiated voltage:

$$\frac{\partial w}{\partial x} = \frac{1}{2\sqrt{2}GSU^2}E_s \tag{3.3}$$

Assuming isotropic turbulence, the rate of dissipation of turbulent energy may then be calculated:

$$\epsilon = \frac{15}{2}\nu\overline{\left(\frac{\partial w}{\partial x}\right)^2}, \tag{3.4}$$

where $\nu \approx 1 \times 10^{-6}\mathrm{m}^2\mathrm{s}^{-1}$ is the kinematic molecular viscosity, and the overline indicates an ensemble average (Lueck et al. 2002).

3.1.3 Acoustic Backscatter

Acoustic backscatter was measured using the Water Column Profiler (WCP). The WCP operated separately from TOMI, recording internally. In order to ensure synchrony, the WCP's internal clock was reset to the time on the ODAS computer before each tow. In addition, the TOMI pressure signal was fed into one of the WCP's auxiliary channels and recorded along with the acoustic data, providing a secondary check of the WCP time (see Section 3.4.3). The acoustic system was calibrated by Tetjana Ross and Rolf Lueck, using a combination of electronic measurements and calibration spheres, at the acoustic test facility at the Institute of Ocean Sciences (Ross 2003).

A typical section of WCP data is shown in Fig. 3.4, and illustrates some of the general properties of the acoustic system and the data it produces. The WCP pings at a rate of 1 Hz, then samples the echo of each ping at a rate of 23.3 kHz. Thus, each ping results in a record of echo intensity as a function of range in front of the transducer (elapsed time from the pulse transmission), up to a maximum range of 20 m. One such record is produced for each ping, so that a two-dimensional array of samples is gradually built up. Within this array, each sample represents the return from the corresponding insonified volume (defined by the sampling rate and the beam width, as discussed below), and is identified by the time it was collected. Using the navigational data recorded by TOMI, corresponding arrays of pressure and distance along the transect are produced, taking into account the motion and attitude of the vehicle (see Section 3.4.3). Thus, each ping is plotted in Fig. 3.4 as a slanted line (due to the pitch of the vehicle), within which each sample is shown as a "pixel". From ping to ping, the towed vehicle moves forward and may change its depth, consequently each ping in Fig. 3.4 starts slightly further along the transect and (in this case) slightly deeper than the previous one.

The data may be further understood by considering the properties of the WCP,

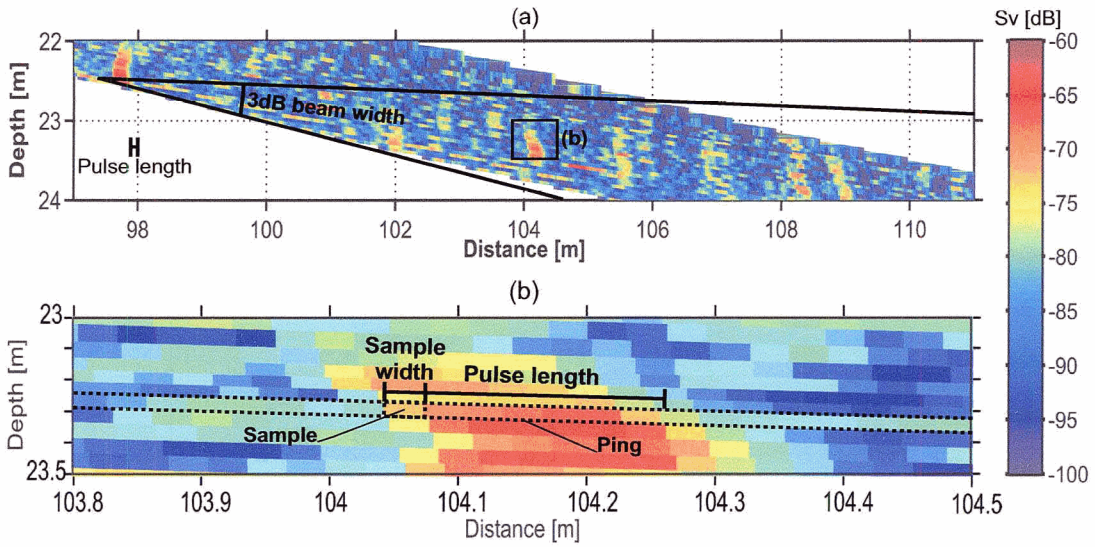

Figure 3.4: Geometry of the WCP data, overlaid on scattering volume data from Fig. 3.3. (a) Beam width and pitch. (b) Sample size and pulse length. The region in (b) corresponds to the box indicated in (a). Note that the the first (closest range) 30 samples (90 cm) of each WCP ping are not shown (transducer ringing).

as described below.

Properties of the Acoustic System

Gain: The WCP's range of sensitivity is determined by the dynamic range of the 8-bit analog to digital converter and by the gain, which was set in the field. With the settings used, target strengths greater than -52 dB ($\sigma_{bs} = 6.1\,\mathrm{mm}^2$) are clipped. In addition to the fixed gain, an approximation to $40log_{10}(r) + 2\alpha r$ time-varying gain, where r is the range from the transducer and α is the acoustic attenuation, is applied by the WCP electronics to account for spreading loss and attenuation (see Section 3.4.3). The lower limit of the system's sensitivity is determined by the electronic noise, discussed below.

Transducer ringing: The WCP begins sampling immediately after transmitting the outgoing pulse. Consequently, the first portion of each recorded ping consists of high-intensity samples corresponding to transducer ringing. After approximately 30 samples (1.3 msec, or a range of 93 cm), valid data is recorded. Typically, these first 30 samples are not shown in images of WCP data (e.g., Fig. 3.4).

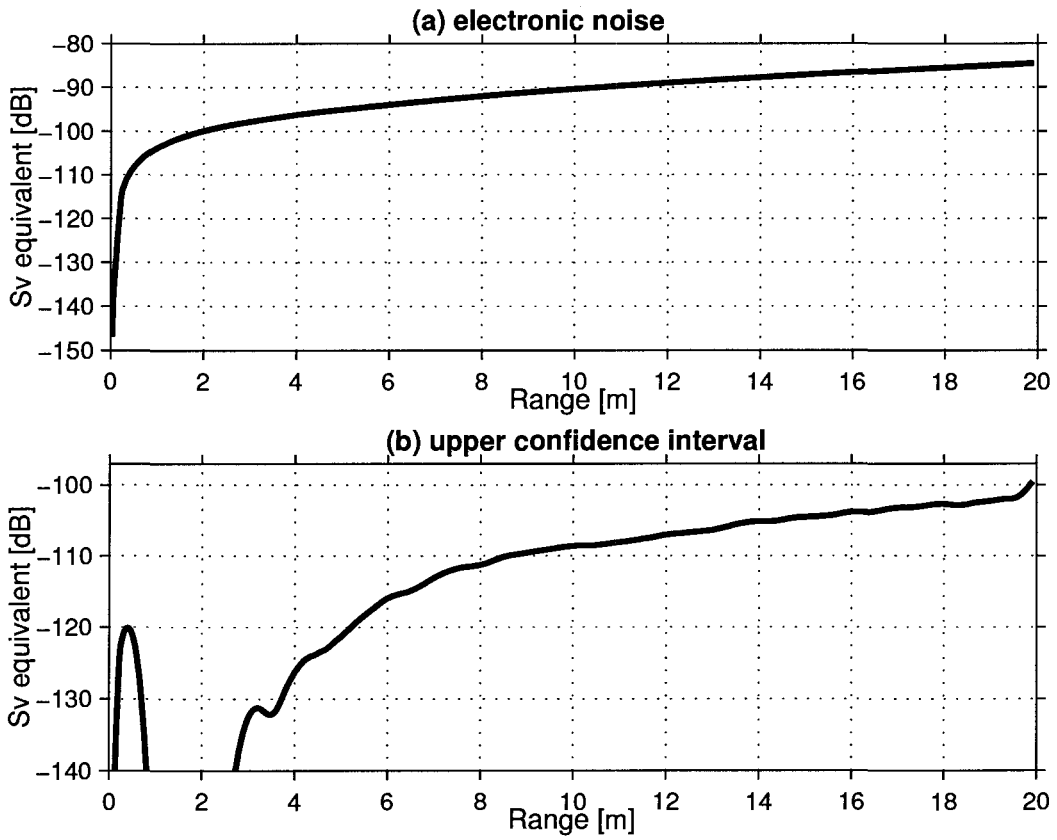

Figure 3.5: Range-dependent electronic noise of the 307 kHz WCP sonar system with the settings most commonly used on the cruise ($C_1 = 0.33\mu F$). (a) Sv equivalent of the electronic noise. (b) Upper 95% confidence interval (by bootstrap approximation, based on lab data), with mean subtracted; the probability that a sample with scattering volume above this curve is due to electronic noise is 5%. The initial peak is due to transducer ringing.

Electronic noise: The electronic noise inherent in the WCP system was measured in the lab by Tetjana Ross and fitted to the TVG curve to yield an average noise curve valid at all ranges (Tetjana Ross, pers. comm.) (Fig. 3.5). There was relatively little ping-to-ping variability in the electronic noise; consequently, after the mean noise has been subtracted from the signal, almost all targets stronger than the curve in Fig. 3.5(b) may be considered "real", i.e. not artifacts related to electronic noise.

Resolution: The sampling rate of the WCP ($f_s = 23.3$kHz) sets its maximum

possible resolution:

$$\Delta d = \frac{c}{2f_s} = \frac{(1445\,\mathrm{m/s})}{2(2.33 \times 10^4\ \mathrm{s}^{-1})} = 3.10\ \mathrm{cm}, \tag{3.5}$$

where c is the speed of sound in water (average value calculated from Knight Inlet CTD data). However, the outgoing pulse is set to a duration of $\tau = 300\mu$s, and so it is considerably longer than this:

$$l = \tau f_s = (3 \times 10^{-4}\ \mathrm{s})(2.33 \times 10^4\ \mathrm{samples/s}) \approx 7\ \mathrm{samples} = 21.7\,\mathrm{cm}. \tag{3.6}$$

This pulse length, set in the WCP firmware, was verified by recording both the transmitted voltage across the transducer and the signal backscattered from a steel sphere in a calibration tank. The significance of this pulse length in terms of the interpretation of acoustic backscatter data is that an object less than 3.10 cm in dimension along the axis of the beam would have an apparent width of approximately 21.7 cm in a WCP image (Fig. 3.4). If the object occupies more than 7 samples in the image, each extra sample represents an increase in dimension of up to 3.10 cm.

Beam pattern: The beam pattern for the 307 kHz transducer is shown in Fig. 3.6. The θ_{-3dB} beam width (shown in Fig. 3.4) is defined as twice the off-axis angle where the sensitivity,

$$\mathrm{S}(\theta) = 20log_{10}\left(\frac{V}{V_0}\right) = 20log_{10}\left(\frac{A}{A_0}\right), \tag{3.7}$$

is -3 dB; here V is the voltage produced by a wave of amplitude A, measured at an angle θ off the transducer axis, and V_0 and A_0 are the values at $\theta = 0°$. $\theta_{-3\mathrm{dB}} = 10°$ for this transducer. While the intensity of objects further off-axis than $\theta_{-3\mathrm{dB}}$ will be greatly reduced, they may still contribute to the observed return. Similarly, the target strength of an object within the beam depends on its angle off-axis. At $\theta = 0°$, the scattering volume is

$$Sv_0 = 20log(A_0) + C, \tag{3.8}$$

where C is a group of corrections discussed in Section 3.4.3. For an angle θ off-axis,

$$A(\theta) = A_0 10^{S(\theta)/20}, \tag{3.9}$$

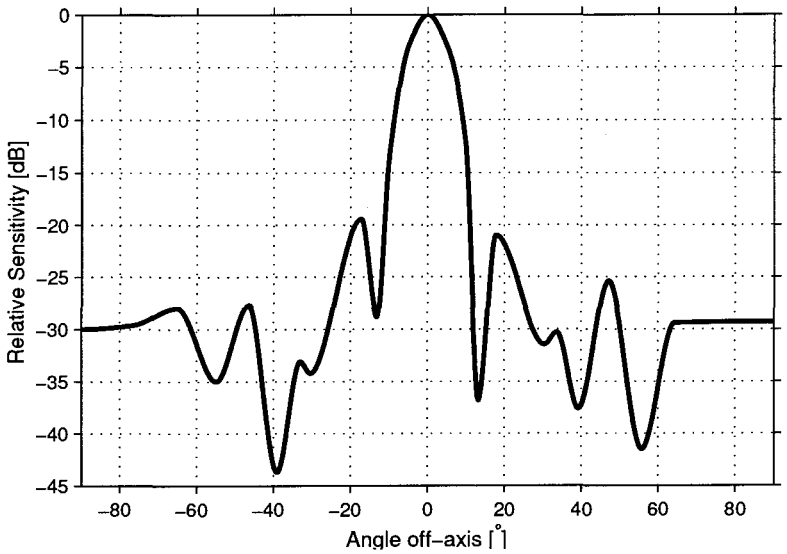

Figure 3.6: Beam pattern for the 307.2 kHz transducer used with the WCP system. The θ_{-3dB} beam width is 10°. Data courtesy of ASL Environmental Sciences Ltd.

and the measured scattering volume is thus

$$Sv = 20log_{10}(A_0 10^{S(\theta)/20}) + C = S(\theta) + Sv_0 \tag{3.10}$$

As a result, approaching targets may become weaker or disappear as they approach the transducer and θ increases. An organism's angle off-axis may also change as a result of its motion. For example, zooplankton may respond to a hydrodynamic disturbance that is perceived as a potential predator by making a fast escape at a moderate angle away from the approach path of the threat (Haury et al. 1980, Ashjian et al. 2002), increasing the off-axis angle.

Insonified Volume

The properties discussed above determine the insonified volume. This volume is bounded by the -3 dB beam width and by the 3.10 cm resolution, and is represented by a single sample in the WCP data (Fig. 3.4). It is described by the following equation:

$$U(r) = \frac{1}{3}\left[\left(r + \frac{1}{4}c\tau\right)^3 - \left(r - \frac{1}{4}c\tau\right)^3\right]\phi, \tag{3.11}$$

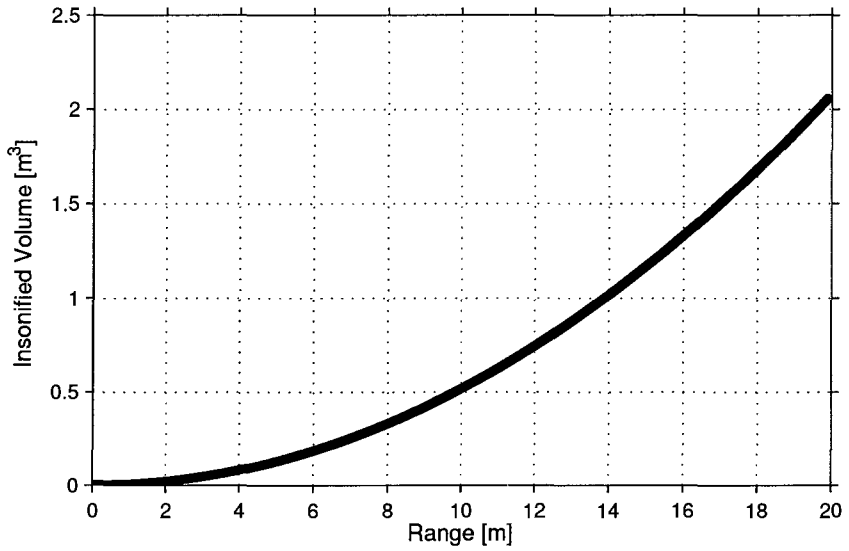

Figure 3.7: Range-dependent insonified volume for a transducer with a pulse length of 300μs and -3 dB beam width of 10°

where r is the range; τ is the pulse duration; c is the speed of sound in water; and ϕ is the equivalent solid angle of the transducer, which can be approximated for a conical beam from the beam width:

$$\phi = 2\pi\left[1 - cos\left(\frac{1}{2}\theta_{-3dB}\right)\right] \tag{3.12}$$

(Vagle et al. 1996). The resulting range-dependent insonified volume is shown in Fig. 3.7. The physical location of each volume may be destermined by its location within a ping, and by the forward motion, depth, and pitch of the vehicle.

The distribution of backscattering cross section within the insonified volume is not known, and will depend on the size of the volume and on the organisms contained in it. This, in turn, affects the interpretation of the scattering volume data, which describe the total backscattering cross-section per unit volume. If the distribution of backscattering cross section within the volume is uniform, the scattering volume is independent of insonified volume and hence range. However, in the more realistic case of an inhomogeneous field, the measurement of scattering volume may be strongly influenced by the inclusion or exclusion of rare, strongly scattering objects, whose target strength will depend on angle off-axis, and hence range. Thus, samples from greater ranges (larger insonified volume, more organisms included) may be con-

sidered to provide information on the average field, whereas samples at closer range (fewer organisms included in the sample) contain more information on smaller-scale structure. In cases where the vehicle is moving more or less horizontally through the water, the result is that the same parcel of water may be sampled acoustically at a number of different scales of averaging.

3.2 Survey Area

The data described in the following chapters were collected around the sill of Knight Inlet (Fig. 3.8), as part of a joint cruise by the Ocean Turbulence Laboratory and the Ocean Physics Group at the University of Victoria. Knight Inlet is a long, narrow glacial fjord, approximately 120 km in length and relatively uniform in width. A remnant moraine near the mouth of the inlet forms a sill at approximately 60 m depth, and separates the deep waters of the Inlet (over 400 m in depth) from the shallower (approximately 150 m), broader outer portion of the inlet. Fresh water enters the inlet from ice fields at its head, principally through the Kliniklini and Franklin rivers (Freeland and Farmer 1980).

Knight Inlet was originally selected as a study site for this cruise for research being conducted by Ross (2003) on the backscattering of sound from turbulent microstructure, based on to the flow patterns that exist around the sill. Similarly, these flow patterns make the sill region interesting biologically. Flow in the Inlet is dominated by the tides, which are mostly semi-diurnal. These have a range from 1 to 4.5 m, and produce an along-inlet displacement of 3 to 6 km (Mackas et al. 2002). The result is a predominantly across-isobath flow around the sill, which varies predictably with time. During the tidal exchange, acceleration of water over the sill under a cap of stratified surface water results in a range of shear levels, and on some tides results in a hydraulic jump as the water plunges over the lee side of the sill (Farmer and Armi 1999). In terms of the work described in the following chapters, a result of these flow conditions is that zooplankton will experience a wide range of turbulent intensities over relatively short spatial and temporal scales.

The zooplankton community in the Inlet includes a variety of organisms, encompassing a wide range of sizes, swimming abilities, and behaviours. The zooplankton biomass in the region is dominated by the euphausiid *Euphausia pacifica*, which has been observed to form dense layers during the day, dispersing at night (Farmer and

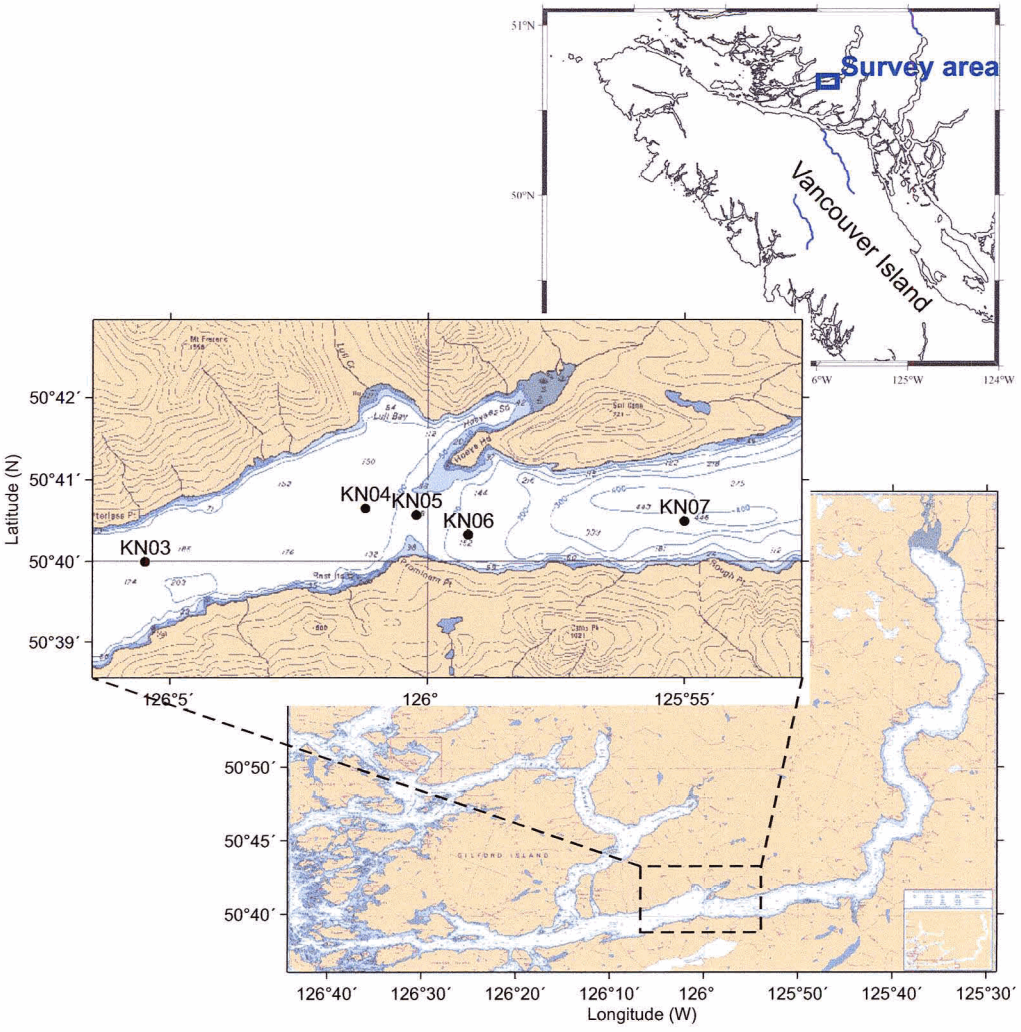

Figure 3.8: Sill area of Knight Inlet, British Columbia. The area enclosed in the boxes and shown in the inset was surveyed in June, 2001. Markers represent CTD/net tow stations.

Date	*Time (PDT)*	*ODAS files*	*WCP file*
21 June	15:20-15:58	KI_2001_2012	KI300_05
21 June	16:58-18:23	KI_2001_2013-2014	KI300_06
21 June	20:20-24:01	KI_2001b_000	KI300_07
22 June	04:39-18:12	KI_2001b_001-004	KI300_08
23 June	05:28-08:42	KI_2001b_2003-2006	KI300_09

Table 3.1: TOMI/WCP tows around the sill of Knight Inlet, June 2001. WCP files 01 to 04, not shown, were used for testing the instrument and setting the gain.

Armi 1999, Trevorrow 2001, Mackas et al. 2002, Mackas, pers. comm.). In addition, a number of copepod species are common around the sill (Stone 1977, Mackas, pers. comm.). Previous research has suggested that the horizontal distributions and interactions of these populations may be strongly influenced by tidal flows (Trevorrow 2001, Mackas et al. 2002, Benfield, pers. comm.), motivating the investigation of effects at sub-metre scales.

3.3 Data Collection

A series of transects were carried out across the sill with TOMI and the WCP, in order to collect data from various stages of the tide over three days (Table 3.1, Fig. 3.9). During each of these tows, the physical and biological variables outlined in Section 3.1 were measured.

During the TOMI/WCP tows, a ship-mounted ADCP (150 kHz) and ship-mounted echosounders (40, 100, and 200 kHz, with the 100 kHz being most useful in identifying scattering layers) collected backscatter and current data. These were used to select depths of interest, which could be targeted by adjusting the depth of the vehicle, and also provided a "big picture" view of zooplankton distributions and the flow environment. Note that due to uncertainties in their calibration, the ship-mounted echosounder data only provide a relative measure of zooplankton backscatter.

Vertical net hauls were done at four stations around the sill using a black SCOR net with 335 μm mesh and a diameter of 56 cm across the opening (Fig. 3.8, Table 3.2). The net was lowered as 0.5 m/s, then retrieved at 1 m/s, collecting organisms during the upcast. These speeds, typically used with the SCOR and similar nets by the Plankton Productivity Group at the Institute of Ocean Sciences, have been found

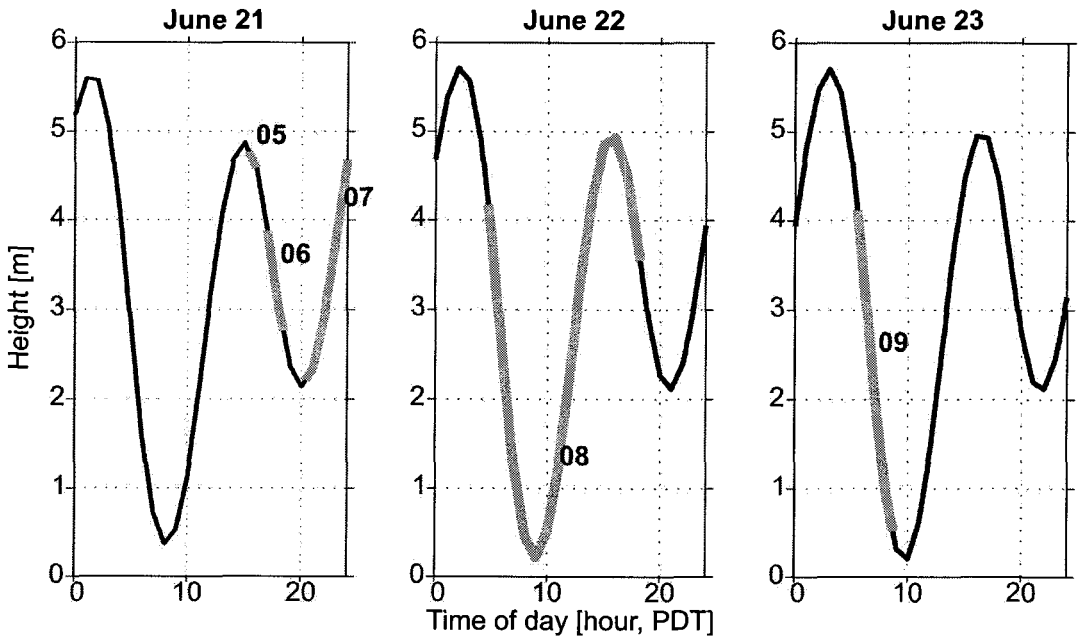

Figure 3.9: Predicted tidal heights in Knight Inlet, British Columbia, and times of TOMI/WCP tows (highlighted and numbered).

to minimize net tangling on the downcast and avoidance on the upcast. The volume of water passing through the net was measured using a flow-meter installed in the mouth of the net, approximately one-third of the way across the diameter. Organisms were washed into the plastic end of the net, and were then preserved in 10% formalin for later analysis.

3.4 Data Processing

3.4.1 TOMI Data

The TOMI data were processed by Tetjana Ross, using routines developed in the Ocean Turbulence Lab; the procedure is described briefly below, and discussed further in Ross (2003).

The TOMI data files were first cleaned, removing any bad data blocks or spurious data points. Further data analysis was then done specific to the variables of interest.

Date	*Station*	*Time (PDT)*	*Depth* [m]
June 20	KN04	07:10	30
		07:25	70
		07:35	145
	KN06	07:55	30
		08:02	70
		08:13	145
June 21	KN04	19:23	80
	KN05	19:42	61
	KN06	19:58	83
June 23	KN03	10:47	120
		10:58	162
	KN04	11:55	135
	KN05	12:15	60
	KN06	12:35	145
	KN07	13:03	100
		13:25	170

Table 3.2: Summary of zooplankton net hauls conducted in Knight Inlet in June, 2001. Stations are numbered increasing eastward, with KN05 at the sill (see Fig. 3.8). All casts are from the depth indicated to the surface.

Pressure and motion data

The pre-emphasized pressure was converted to a high-resolution pressure by low-pass filtering with a first-order Butterworth filter, as described in Mudge and Lueck (1994). The pressure and motion signals were then converted to physical units using previously determined calibration coefficients.

The distance between the ship and TOMI was approximated based on the amount of wire let out from the spool and the wire angle, and was later used to lag the WCP data with respect to the ship-mounted acoustic data.

After calibration, the accelerometer and gyro data were used to calculate the pitch, roll, and yaw of the vehicle.

Fine-scale temperature, salinity, and fluorescence

The Sea-Bird temperature and conductivity data were calibrated using calibration data obtained from Sea-Bird Electronics Inc. in September, 2000.

The fluorescence was converted to a voltage based on the 20V range of the 16-

bit A/D converter. Conversion to a concentration of chlorophyll requires calibration using a similar species assemblage to that encountered in the field; as this was not practical, the voltage was used as a relative measure of chlorophyll concentration.

Microscale temperature

The pre-emphasized temperature data were de-emphasized as described above for the pressure signal, then calibrated by comparison with the fine-scale Sea-Bird temperature data, yielding a high-resolution temperature signal in physical units. These data were also used to calculate small-scale temperature gradients, $\frac{dT}{dx}$.

Dissipation rate

Shear data were first cleaned and converted to physical units. Contamination of the data, due to vibrations or to particles hitting the probes, was removed. Particle hits, which occur as spikes in the data, were found by comparing the record to a smoothed version of the absolute value; points more than 8 times higher than the smoothed record were removed, along with 11 neighbouring points on either side (to eliminate ringing). This despiking process removes less than 0.01% of the data. Vibrations, observed at vehicle speeds over about 1.7 m/s (representing about 2% of the data (Ross 2003)), are recorded in the accelerometer data. Filtering using Wiener optimal filters with respect to the port-starboard and then vertical accelerometers removed that part of the shear signal that was coherent with the accelerometer signal. The resulting signal was then converted to physical units using previously determined calibration coefficients.

The shear data were then used to calculate the turbulent energy dissipation rate ϵ, using equation 3.4. One-second FFT's were calculated on the cleaned shear data and averaged over 10 second sections of data. These spectra were corrected for signal attenuation at scales smaller than the dimensions of the shear probe using the single-pole model described in Macoun and Lueck (2004). The shear variance $\overline{(\frac{\partial w}{\partial x})^2}$ for each 10-second data section was then calculated by integrating the shear spectrum up to the transition from signal to noise at high wavenumbers, and used to yield an initial estimate of the dissipation rate. This dissipation rate estimate was then adjusted by comparison with the Nasmyth spectrum, thus compensating for variance missed at high wavenumbers (Nasmyth 1970, Macoun 2003).

3.4.2 Zooplankton Net Tows

The formalin-preserved samples were sorted and counted by Moira Galbraith. Large organisms (> 5mm) were counted and removed, either in the whole sample or in a fraction as small as 1/4. The remaining sample was split using a Folsom splitter, so that counting was done on a reasonable fraction of the sample, between 1/128 and 1/32, or roughly 500-1000 individuals. Organisms in the sub-sample were sorted into genera (or species where possible) and life stage, and then counted. The counts were converted to number per cubic metre based on the volume of water sampled (from the flow-meter readings). As each category of organism has a characteristic length scale (see Appendix A), size distribution data can thus be obtained.

Because the SCOR net is not a closing net, only data for depth intervals including the surface are directly obtained by the above process. In order to obtain estimates for given depth ranges, sets of stratified casts were done at stations KN04 and KN06 on June 20, and at KN03 and KN07 on June 23 (Table 3.2). The densities of organisms in the shallower nets were then subtracted from those in the deeper nets to produce estimated densities for depth intervals (e.g., $30 - 70$ m on June 20). This was done separately for each taxon listed in Appendix A, setting negative values to zero. This approach is valid if the zooplankton field does not change significantly in the brief time required to conduct the casts. In particular, the similarity (in terms of species composition) between two samples from the same depth must be greater than the similarity between samples from different depths; this is supported by the nets from Knight Inlet, and by similar work by Benfield et al. (1996).

3.4.3 Acoustic Data

Visual quality control of the WCP data was first done by plotting the raw data. The pressure signal was also plotted against that recorded by ODAS as a check of the synchronicity between the ODAS and WCP clocks; the two were found to be in good agreement.

The following corrections were applied to the raw acoustic data:

1. A shift of 5 counts was added to the 307 kHz data (full range is 0-255 counts) to correct for a downward shift produced by the 8-bit analog to digital convertor in the WCP.

2. The average range-dependent electronic noise curve (see Section 3.1.3) was subtracted from the WCP data, such that the data represent the mostly noise-free signal.

3. As part of the sonar equation (see below), a correction is made to account for differences between the time-varying gain applied by the electronics and the ideal, physical form.

Once the first two of these corrections were applied, the raw counts were converted to physical units using the sonar equation:

$$Sv = 20log_{10}(A) + K + 40log_{10}(r) + 2\alpha r - TVG(r) - 10log_{10}(U), \qquad (3.13)$$

where $Sv = 10log_{10}(\sigma_{bs})$ is the scattering volume (in dB), A is the raw acoustic return, in counts (proportional to voltage), K is the calibration coefficient, α is the acoustic attenuation of seawater, $TVG(r)$ is the range-dependent time-varying gain (produced by the electronics), and U is the insonified volume (see section 3.1.3). $40log_{10}(r)+2\alpha r$ is the predicted time-varying gain for reflection from a single object, and accounts for both spreading loss and attenuation. $\alpha = 0.0689\,\mathrm{dB/m}$ was calculated from François and Garrison (1982), using typical values of temperature, salinity, and pressure.

The motion data collected by TOMI were used to convert the temporal co-ordinates in which the WCP data were collected (time along a single ping, time between successive pings) to spatial co-ordinates (distance along the transect, depth). The depth of the vehicle (recorded by TOMI's pressure transducer) and its forward motion (based on flow-meter data) were used to locate the vehicle at the start of each ping, and the location of samples within each ping was determined from the speed of sound in seawater ($c = 1445\,\mathrm{m/s}$ for average temperature and salinity in Knight Inlet) and the pitch of the vehicle (yaw and roll were found to have a negligible effect) (Fig. 3.4). Typically, TOMI's pitch was fairly small (less than 5°), and corresponded to the angle of the vehicle path; i.e., the acoustic beam was generally pointed at least roughly in the direction of motion. However, in cases where a steep angle of descent was produced in TOMI by allowing the tow cable to become slack (by letting out additional cable and/or reducing ship's speed), the angle of descent was sometimes greater than the pitch (e.g., Fig. 4.12(b)).

Chapter 4

Observations

4.1 Physical and Biological Environment

4.1.1 Flow Over the Sill

The large tides of June 21-23 were characterized by high flow speeds and shear levels around the sill (Fig. 4.1). During the ebb tide, fast-flowing water moving over the steeper western side of the sill was capped by a slower-moving stratified layer; this produced high shear levels near the surface and in the lee of the sill, with lee waves during the larger ebbs (Fig. 4.1(a)). Flow during the flood tide was less compressed due to the deeper, more gently sloping eastern side of the sill, consequently lee waves were not observed. However, flow speeds were similar to those observed during the ebb, and high levels of shear were observed near the surface (Fig. 4.1(b)).

Dissipation rates measured during the large tidal cycle illustrated in Fig. 4.1 varied from 8×10^{-10} to 3×10^{-4} W kg^{-1}, with the highest dissipation rates occurring in the lee wave formed during the strong ebb (Fig. 4.2). The average dissipation rate observed during the peak flows illustrated in Fig. 4.2 (1×10^{-5} W kg^{-1} and 5×10^{-6} W kg^{-1} for the ebb and flood, respectively) was one to two orders of magnitude greater than that near slack tide (2×10^{-7} W kg^{-1}).

Mixing of the stratified surface layers resulted in steep horizontal gradients in temperature (dT/dx) during some stages of the tide (Fig. 4.3). In such regions, backscatter from temperature and salinity microstructure may become an issue (Section 2.2; Ross 2003, Ross and Lueck 2003). While the strongest gradients occurred near the surface (i.e., shallower than approximately 35 m), moderately high values of dT/dx

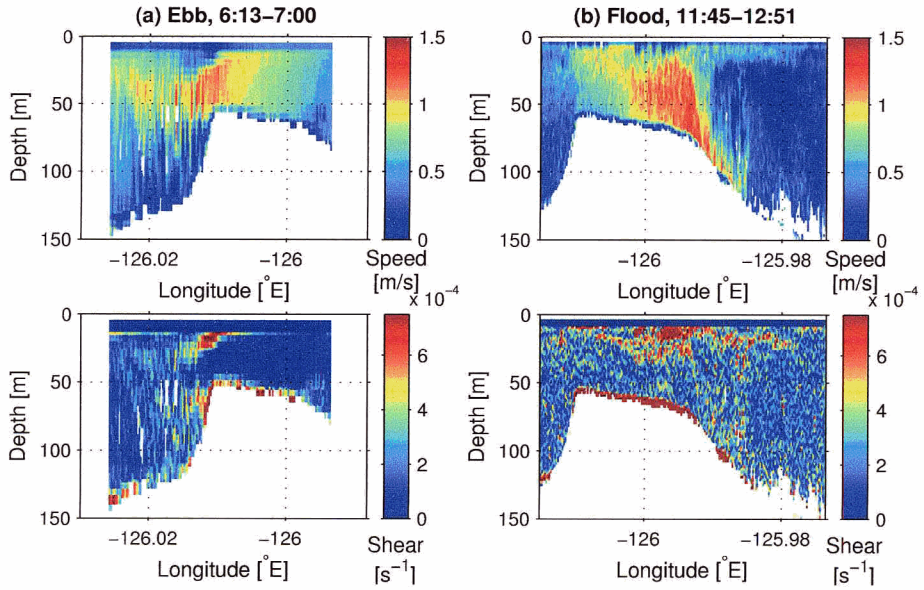

Figure 4.1: 150 kHz ship-mounted ADCP data collected during the larger ebb and flood on June 22, 2001. Upper panels: horizontal current speed. Lower panels: vertical shear.

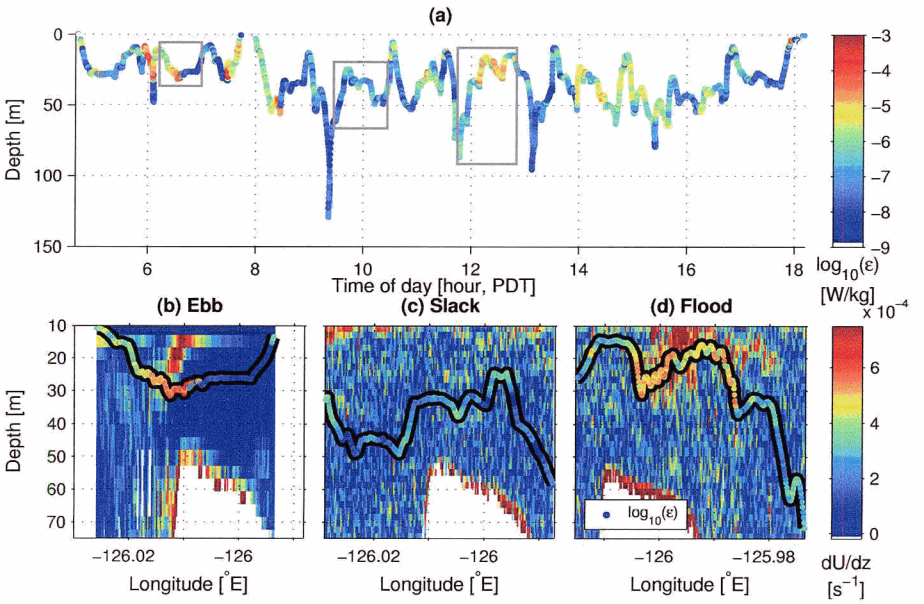

Figure 4.2: Dissipation rate data collected around the sill of Knight Inlet on June 22, 2001. Boxed regions in (a) are reproduced in the lower panels (b-d) over the corresponding 150 kHz ADCP shear data, with the same colour coding as in (a). Note that the ship was travelling eastward in (b), and westward in (c) and (d).

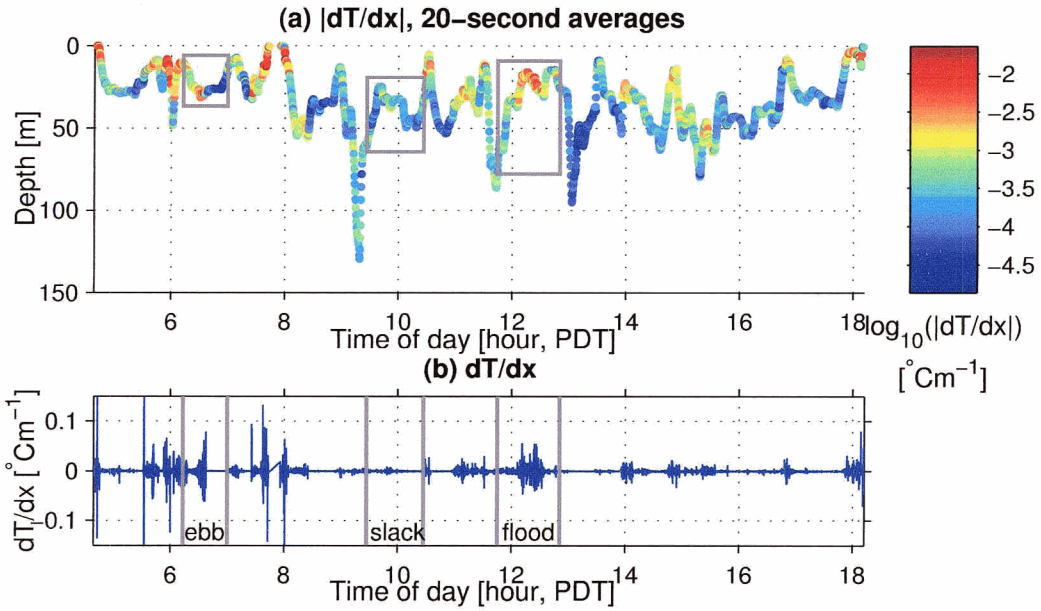

Figure 4.3: Horizontal microstructure temperature gradients around the sill of Knight Inlet on June 22, 2001. Boxed regions in (a) are reproduced in (b).

were observed at greater depths during strong tidal exchanges (e.g., approximately 15:30 in Fig. 4.3).

4.1.2 Phytoplankton and Zooplankton

Concentrations of phytoplankton were highest in the well-lit surface layer (shallower than 35 m), and quickly decreased with depth (Fig. 4.4). The non-motile phytoplankton appeared to be advected and dispersed by the tide, consistent with the flow patterns observed with the ADCP (Figs. 4.1, 4.4).

The bulk of daytime zooplankton backscatter was observed below sill depth (Fig. 4.5). Two scattering layers were regularly observed during quiescent periods (Fig. 4.5(b), see also Fig. 4.9): a faint layer around 65 m depth, and a strong layer around 100 m (typically seen on the west side of the sill). The layers exhibited diurnal migration patterns, moving up to the surface or spreading out throughout the water column during the night, and returning to depth at dawn. In addition, regions of stronger scatter were sometimes observed near the bottom on the west side of the sill (e.g., along the bottom in Fig. 4.5(b)). Schooling fish were also present in the area,

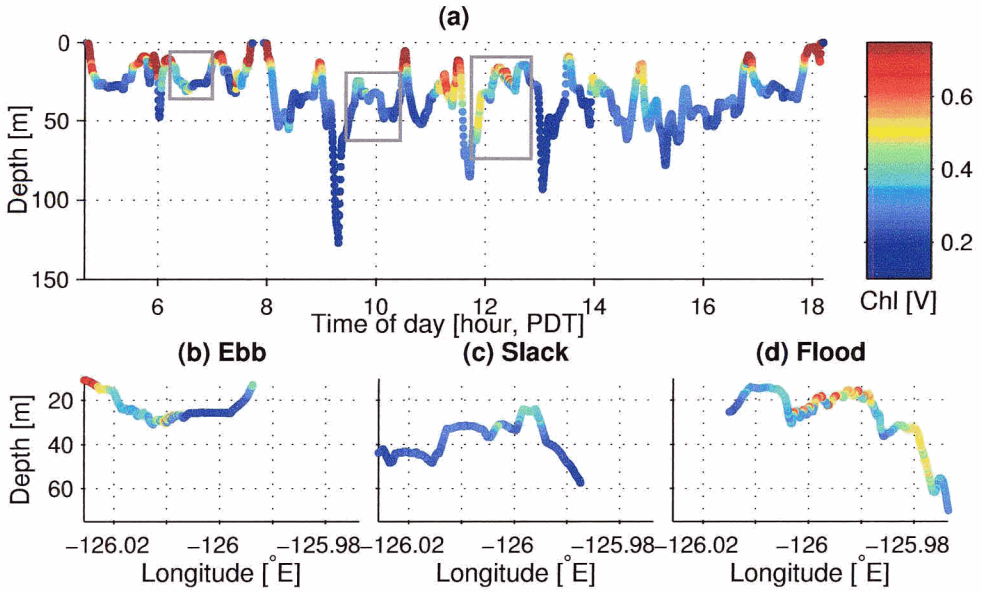

Figure 4.4: Chlorophyll fluorescence measured around the sill on June 22, 2001 (subsampled to 0.05 Hz). Boxed regions in (a) are reproduced in the lower panels (b-d). Top of the sill is located between approximately 126.01°W and 125.98°W. Note that the ship was travelling eastward in (b), and westward in (c) and (d).

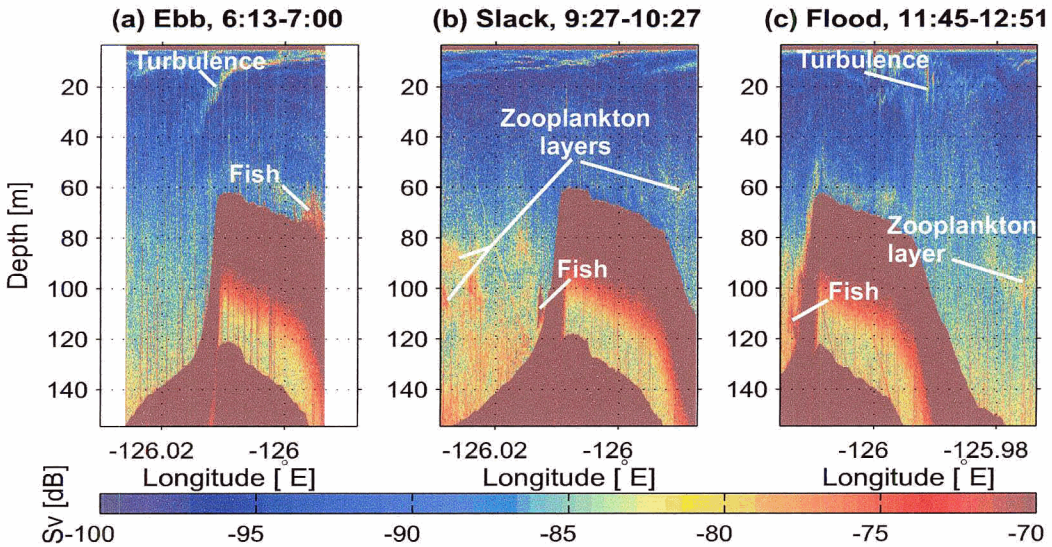

Figure 4.5: 100 kHz ship-mounted echosounder data collected around the sill of Knight Inlet on June 22, 2001. Probable sources of scatter are labelled. Vertical lines and increased scatter at greater depth are instrumental artefacts. Note that calibration of the echosounder is approximate.

and are likely responsible for the strongest returns (-70 dB and higher) observed (e.g., approximately 110 m on the west side of the sill in Fig. 4.5(b)).

As current speeds increased, these layers disappeared in the immediate vicinity of the sill. During the ebb tide (Fig. 4.5(a)), the downstream zooplankton scattering layer disappeared, while the upstream layers (not shown in the figure) remained. During the flood tide (Fig. 4.5(c)), the downstream scattering layer was again disrupted, although to a lesser extent, with the layer reforming at a short distance from the sill. In each case, a region of strong scatter, possibly associated with fish, was observed against the upstream slope of the sill. Although some scatter can be seen in high-shear surface regions during both tides, this is likely the result of bubbles and temperature/salinity microstructure rather than zooplankton (Ross 2003).

Zooplankton samples collected with the nets were dominated numerically by small organisms, mainly copepods (Fig. 4.6; see also Appendix A) (note that most organisms in the "Other" category of Fig. 4.6(b) are either very small overall or very slender, < 1 mm). This was particularly true in the near-surface regions (< 30 m), which were characterized by high densities of copepods approximately 1 mm in length, as well as variable abundances of pteropods, larvaceans, and chain-forming phytoplankton.

Mid-water (30-80 m), larger copepods (2-4 mm) were dominant. Juvenile euphausiids (6-7 mm) and amphipods (≈ 4 mm) also occurred in varying numbers, with amphipods becoming more common deeper than approximately 70 m; when acoustic scattering layers within this depth range were sampled, these two groups were usually found in elevated abundances. Deeper still, samples generally contained a large proportion of medium to large amphipods, copepods, and euphausiids, and were much more likely to include organisms approaching a centimetre or more in size. Adult euphausiids (11-22 mm) were commonly found in the deeper net casts, and occurred in higher numbers when the scatter layer at approximately 100 m depth was sampled. The largest size classes (up to 25 mm) were only captured in the deepest cast on the west side of the sill on June 20; these may explain some of the near-bottom backscatter in that region.

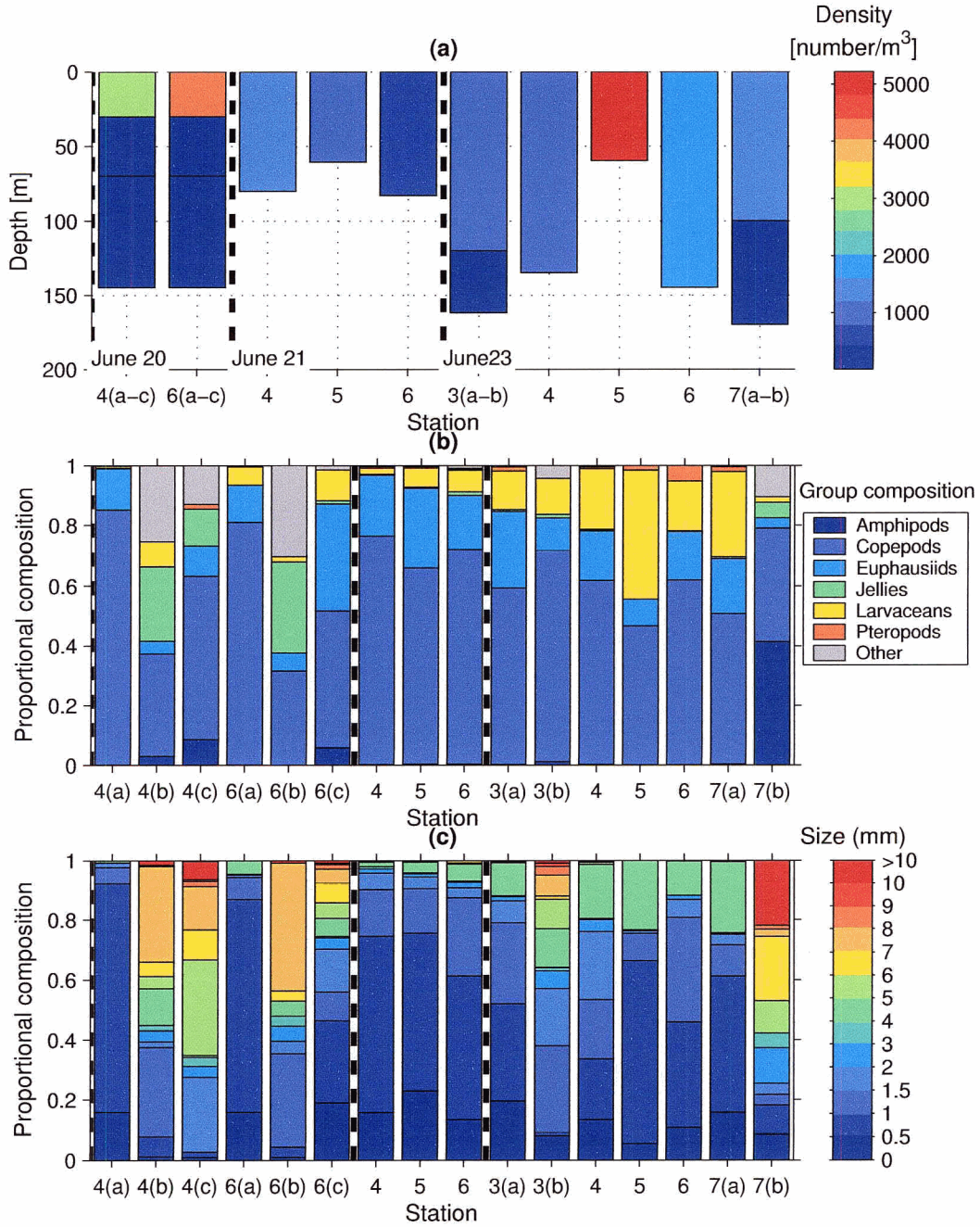

Figure 4.6: Zooplankton samples collected in Knight Inlet in June, 2001. Estimates for deeper intervals were produced by subtracting shallower casts from deeper ones in series of net hauls at the same time and location (see Section 3.4.2).

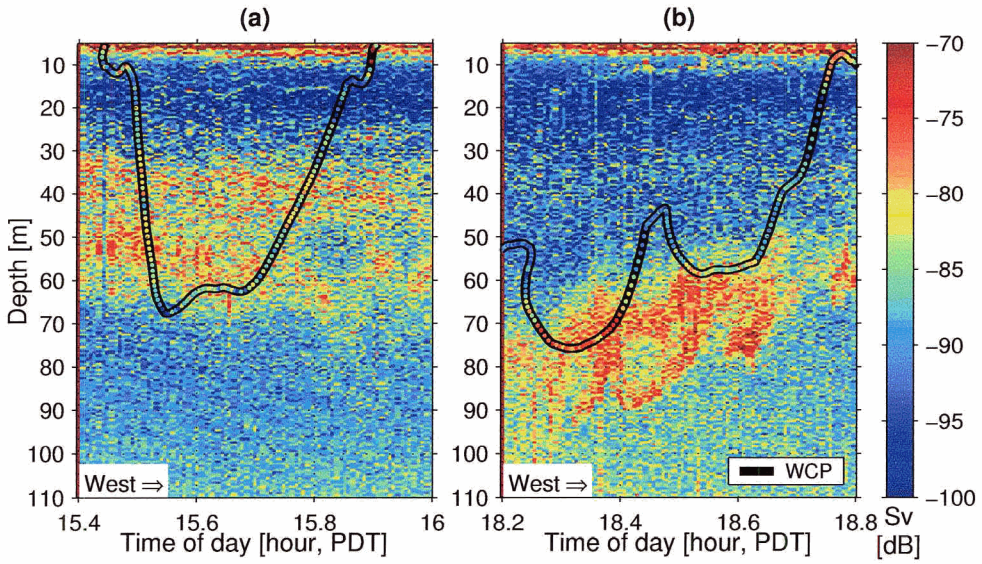

Figure 4.7: Ship-mounted echosounder (100 kHz) and WCP (307 kHz) measurements of scattering layers observed on the east (a) and west (b) sides of the sill on June 21, 2001. WCP data, plotted as coloured circles against a black line, were averaged between 15 and 16 m range in front of the vehicle, and shifted in time to match the location of the ship-mounted data; for clarity, only every tenth point is shown. The background image in each panel is from the ship-mounted echosounder.

4.2 WCP Scattering Volumes

4.2.1 Ship-Mounted vs. Towed Acoustics

Although direct comparisons cannot be made between scattering volumes measured by the 100 kHz ship-mounted echosounder and the 307 kHz WCP, the former was used to locate stable acoustic scattering layers, which were then sampled by the WCP up to 8.7 minutes later (Fig. 4.7). In such regions, the WCP agreed well with the echosounder with respect to the depth, vertical extent, and relative strength of the scattering layers, supporting further comparisons with zooplankton data.

4.2.2 Predicting Acoustic Backscatter from Net Data

Application of the Models

Predictions of acoustic backscatter were calculated from the number densities and size distributions of copepods, amphipods, euphausiids, and pteropods captured in the nets, using equations 2.14 and 2.15 (see Appendix A for a detailed list of species and sizes within each of these groups). These taxa were numerically dominant, large enough to significantly influence total backscatter, and well described in the literature. By comparison, the following groups were expected to make negligible contributions to total backscatter:

- Siphonophores and jellies: Siphonophores captured in Knight Inlet in June, 2001, were not gas-bearing, hence low returns are expected from both groups due to low compressibility and sound-speed contrasts between their tissues and seawater (Stanton et al. 1994, Mutlu 1996).

- Larvaceans: Few acoustic parameters exist in the literature, but most of these small organisms' volume consists of a large mucous feeding structure; as with jellies, this low-contrast structure is expected to be very weakly scattering.

- Other: The small sizes and low number densities of these organisms produced a negligible contribution to backscatter (less than 1% of the combined backscatter from copepods, euphausiids, and amphipods when modelled as fluid spheres).

As a result of their hard shells, pteropods dominated the total backscatter for net casts which sampled the near-surface layer (Fig. 4.8), and accounted for much of the variability in the predicted scattering volumes. The total contribution from the three fluid-like taxa varied over a smaller range, although the relative importance of each group changed from tow to tow. The total backscatter from these taxa in general, and from euphausiids in particular, was usually higher when mid-water acoustic scattering layers were sampled (Fig. 4.9). Moderately-sized organisms (5-7 mm) from each taxon made the largest contributions to total backscatter, with abundant small organisms playing a relatively minor role (Fig. 4.8(b,d)).

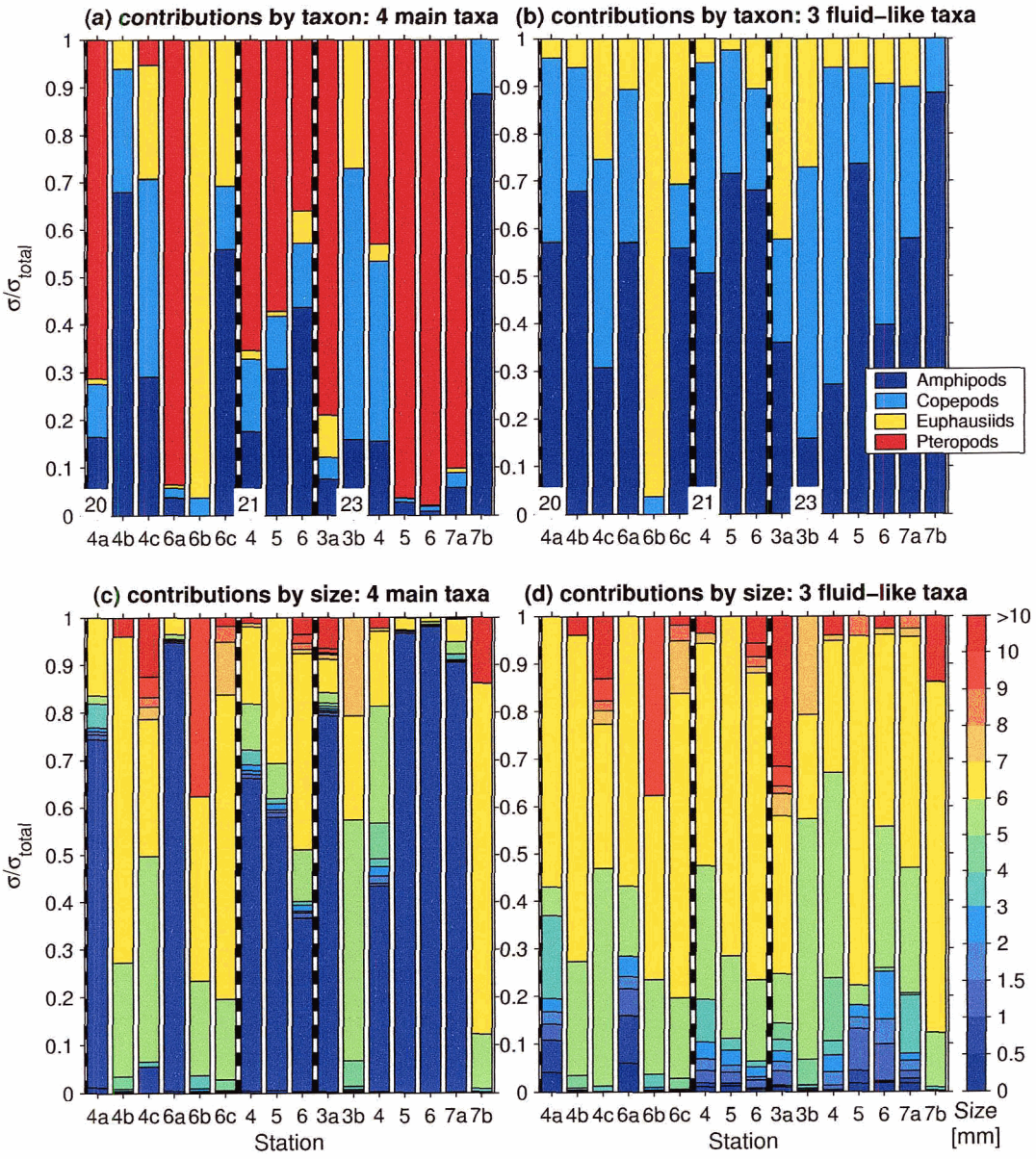

Figure 4.8: Contributions to the total back-scattering cross-section predicted from net haul data, by taxon (a-b) and size distribution (c-d). Dates in June, 2001, are labelled at the bottom of the top panels. Station labels are as in Fig. 4.6, with the station number followed by a,b,c where more than one depth range was sampled (see also Table 3.2). Contributions from only the three fluid-like taxa (i.e., excluding gastropods) are shown in the right-hand panels.

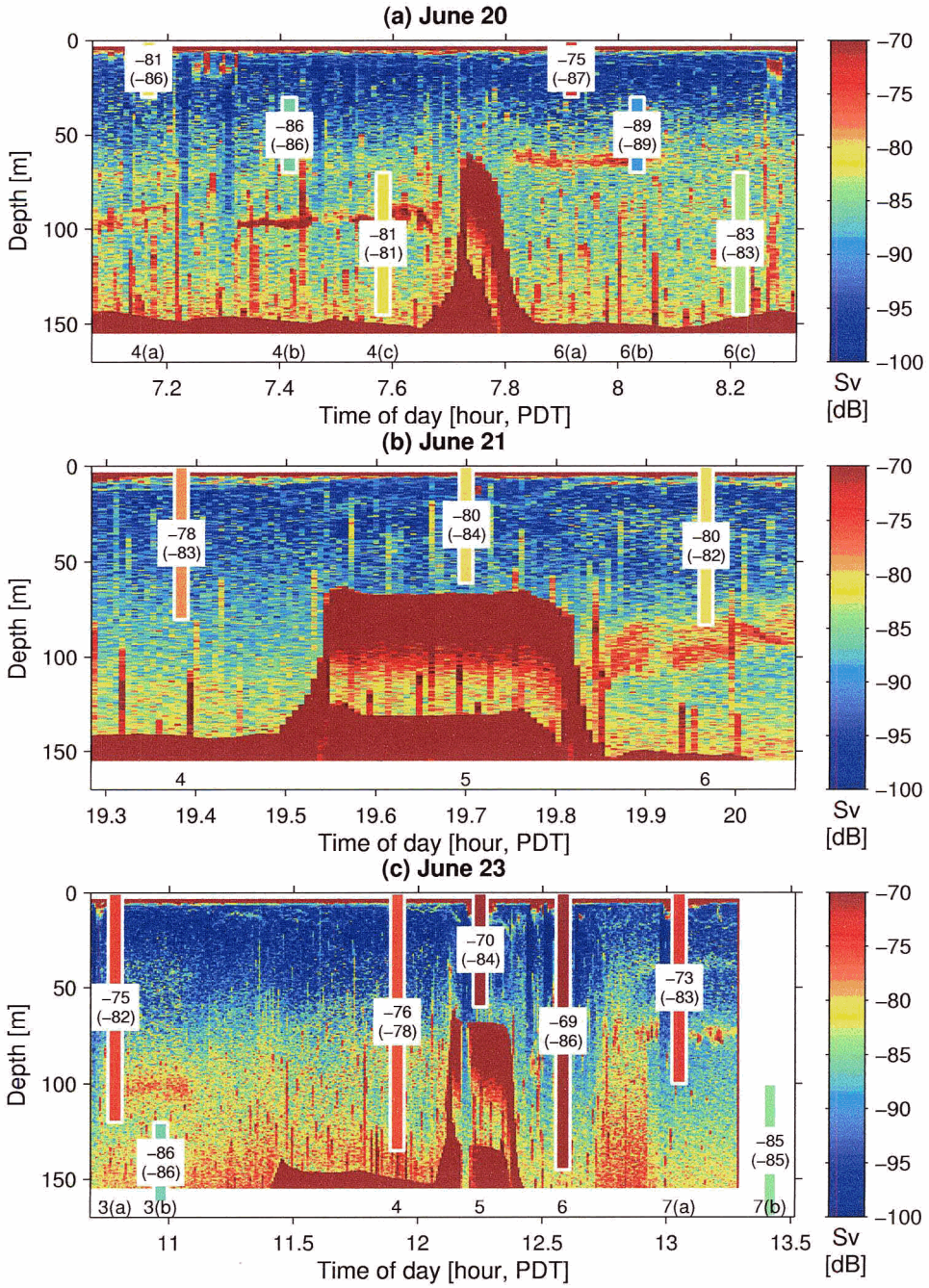

Figure 4.9: Location of zooplankton net casts (plotted over 100 kHz ship-mounted echosounder data) and predicted backscatter at 307 kHz due to copepods, amphipods, euphausiids, and pteropods; backscatter from only the first three groups is shown in parentheses. Station numbers are labelled at the bottom of each panel.

Station	*WCP section*			*Net cast*		
	Label	*Depth range [m]*	$\overline{Sv}$ *[dB]*	*Date/time (PDT)*	*Depth range [m]*	*Predicted Sv [dB]**
KN05	(a)(1)	13-55	-89	21/19:42	0-61	-80 (-84)
	(a)(2)		-89	23/12:15	0-60	-70 (-84)
KN06	(b)	13-30	-89	20/07:55	0-30	-75 (-87)
	(c)	30-70	-84	20/08:02	30-70	-89 (-89)
	(g)		-85			-89 (-89)
	(d)	13-83	-86	21/19:58	0-83	-80 (-82)
	(e)	70-128	-87	20/08:13	70-145	-83 (-83)
	(f)		-86			-83 (-83)
KN04	(h)	10-30	-87	20/07:10	0-30	-81 (-86)
	(i)		-83			

Table 4.1: Depth ranges and scattering volumes for WCP data collected near slack tide on June 22, 2001 (Fig. 4.10), and predicted scattering volumes from matched net casts. (*contributions from the fluid-like taxa are shown in parentheses)

Extraction of WCP Data

Sections of WCP data with relatively constant rates of ascent or descent were chosen from locations, depths, and flow speeds similar to those sampled by the nets (e.g., Fig. 4.10). While depth ranges similar to those sampled by the nets were used whenever possible, slightly different ranges had to be used in some cases (e.g., the WCP cannot sample up to the surface due to surface reflections and bubbles in the ship's wake). For each section of WCP data selected, the scattering volume at 3 m range in front of the transducer was averaged over the appropriate depth interval. At this range the electronic noise is relatively low (Fig. 3.5), the insonified volume is small (0.047 m^3), and avoidance due to hydrodynamic disturbance by the instrument and tow cable should be minimal. In order to minimize the potential for interference from turbulent backscatter, only sections from near slack tide are discussed here ($\overline{\epsilon} \leq 1.5 \times 10^{-7}$ W kg^{-1} and $\overline{dT/dx} \leq 0.03$ °Cm^{-1} for the sections shown in Fig. 4.10); scattering volumes in such regions were not correlated with dT/dx, and the backscatter measured by the WCP should be due to zooplankton.

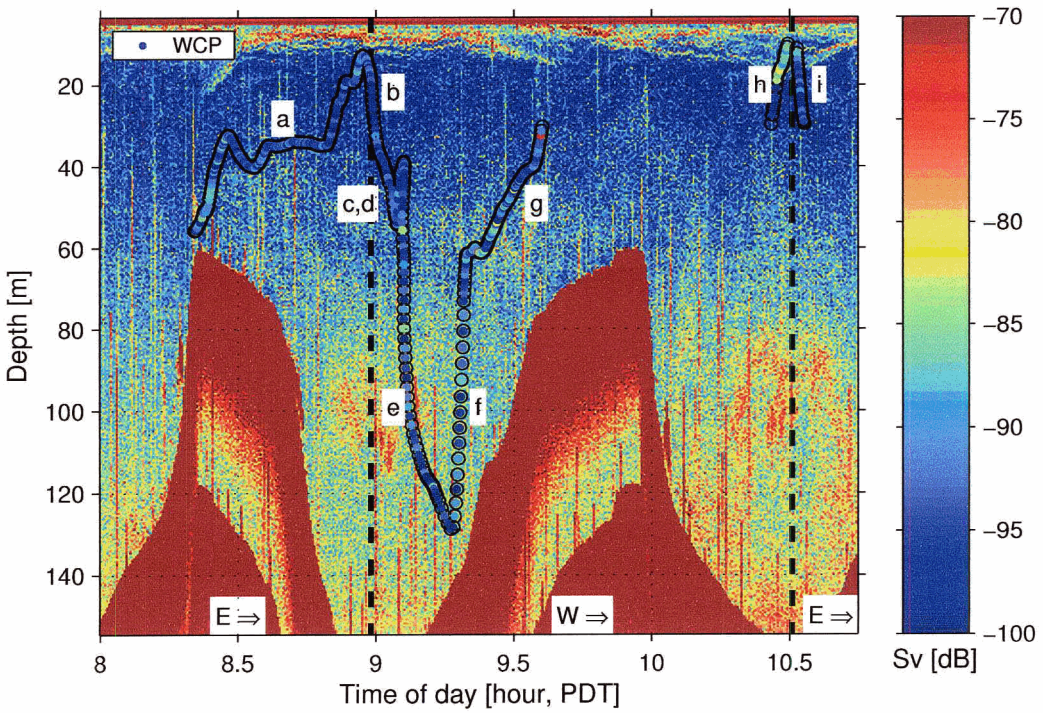

Figure 4.10: Sections of WCP backscatter data used for comparison with predictions from net tows, plotted over 100 kHz ship-mounted echosounder data. WCP scattering volumes are averaged between 2.5 and 3.5 m in front of the transducer. WCP data are shown as coloured circles; for clarity, only every tenth point is plotted. Labels refer to Table 4.1; vertical dashed lines indicate turns.

Comparison with WCP Data

The average scattering volumes measured by the WCP and predicted by the nets each varied over several dB (Fig. 4.9, Table 4.1). In the nets, this was due in large part to the importance of pteropods, whose abundances differed by an order of magnitude between similar casts on opposite sides of the sill or on different days. Variability among similar regions was greater still in the WCP data, which may have been more sensitive to small-scale patchiness and rare scatterers than the nets. Similarly, the average scattering volumes predicted from the nets often differed considerably from the values measured in similar regions by the WCP, and it was not possible to correlate the two sets of measurements (Table 4.1). However, the differences between the measured and predicted scattering volumes were within the range of variability seen among similar WCP sections. In particular, the magnitude of the differences were

not unrealistic considering that nets and WCP data were collected on different days. Furthermore, the nets did not appear to systematically over- or under-estimate scattering volumes in regions where turbulence was not a significant source of backscatter (note that while the WCP scattering volumes shown in Table 4.1 tended to be lower than the net estimates, this was not consistently the case when other sections of WCP data were considered).

Based on the observation that the average scattering volumes predicted from the nets were on the same order as those measured by the WCP, the distributions of target strength obtained from these two types of measurements were also compared. Histograms of target strength were computed for the nets and for sections of WCP data such as those listed in Table 4.1, and the net histograms were used for a target-by-target accounting of the WCP data. Starting with histograms such as those shown in the left-hand panels of Fig. 4.11, the net and WCP data are compared as follows:

1. Starting with the highest-TS bin in the WCP histogram, the net data are used to attempt to account for the number of WCP returns at this intensity. If the net contained organisms of the same target strength, these are used first, with one organism being used to account for one WCP sample. The total backscatter from these organisms (equal to that from the WCP) is shown in red in the right-hand panels of Fig. 4.11. If any of these organisms are left after accounting for all WCP targets of a given target strength, they may be used in a later step to account for weaker WCP returns.

2. If not enough organisms were present in the net to explain all WCP returns of a given target strength on the one-to-one basis outlined in Step 1, then the WCP returns that remain unaccounted for must be the sum of the backscatter from two or more organisms. The number of organisms of target strength TS_1 required to explain a single WCP target of strength TS_2 is

$$N = \lceil 10^{(TS_2 - TS_1)/10} \rceil. \tag{4.1}$$

Note that the ceiling function (denoted by "$\lceil\rceil$") is used to avoid using parts of organisms; however, similar results are obtained if N is not rounded. Such groups of organisms are used to account for the WCP targets, until all WCP returns in the bin under consideration have been accounted for or no net or-

ganisms remain. The backscatter from these organisms is shown as blue bars in the right-hand panels of Fig. 4.11.

3. The above two steps are then repeated with the next highest bin in the WCP histogram, and so on for the rest of the histogram.

The total WCP backscatter may then be plotted as the sum of three parts (Fig. 4.11(b,d,f)): (1) the portion that may be accounted for using individual organisms (shown in red); (2) the portion that must be accounted for as groups of organisms (shown in blue); and (3) that portion which is left unaccounted for after all net organisms have been "used up" in accounting for higher-intensity WCP returns (shown in yellow).

A central assumption in this comparison is that the WCP targets are most likely to represent either single organisms or aggregations of the smallest possible number of organisms. While larger aggregations of more weakly scattering organisms are physically possible, explaining a strong target in terms of a swarm of considerably more weakly scattering organisms would require local densities much higher than those observed in the nets. There is also likely to be a "background" of small (< 1 mm), very common, organisms in each insonified volume; however, the total backscatter from such organisms is very low (Fig. 4.8), and does not significantly affect calculations involving larger organisms.

It should be noted that while this approach can yield a first-order approximation to how well the WCP backscatter can be explained in terms of the organisms captured in the nets, the number of assumptions and approximations involved, combined with the temporal separation between the net and WCP data, make this approach unsuitable as a detailed accounting of a specific section of WCP data. In particular, it is likely to be highly sensitive to differences in the zooplankton communities sampled by the particular net and WCP sections being compared. For example, if the net includes many more strong scatterers than the WCP data, these may have to be used to explain WCP targets with considerably lower target strengths. An example of this is shown in Fig. 4.11(a), for which the net contained a large number of pteropods ($TS = -86$ dB). As there was no correspondingly large number of strong WCP samples, these had to be used to explain WCP returns with a lower target strength, and as a result a portion of the WCP data was left unexplained despite the high scattering volume predicted from the nets. Similarly, the low total scattering volume observed in the net depicted

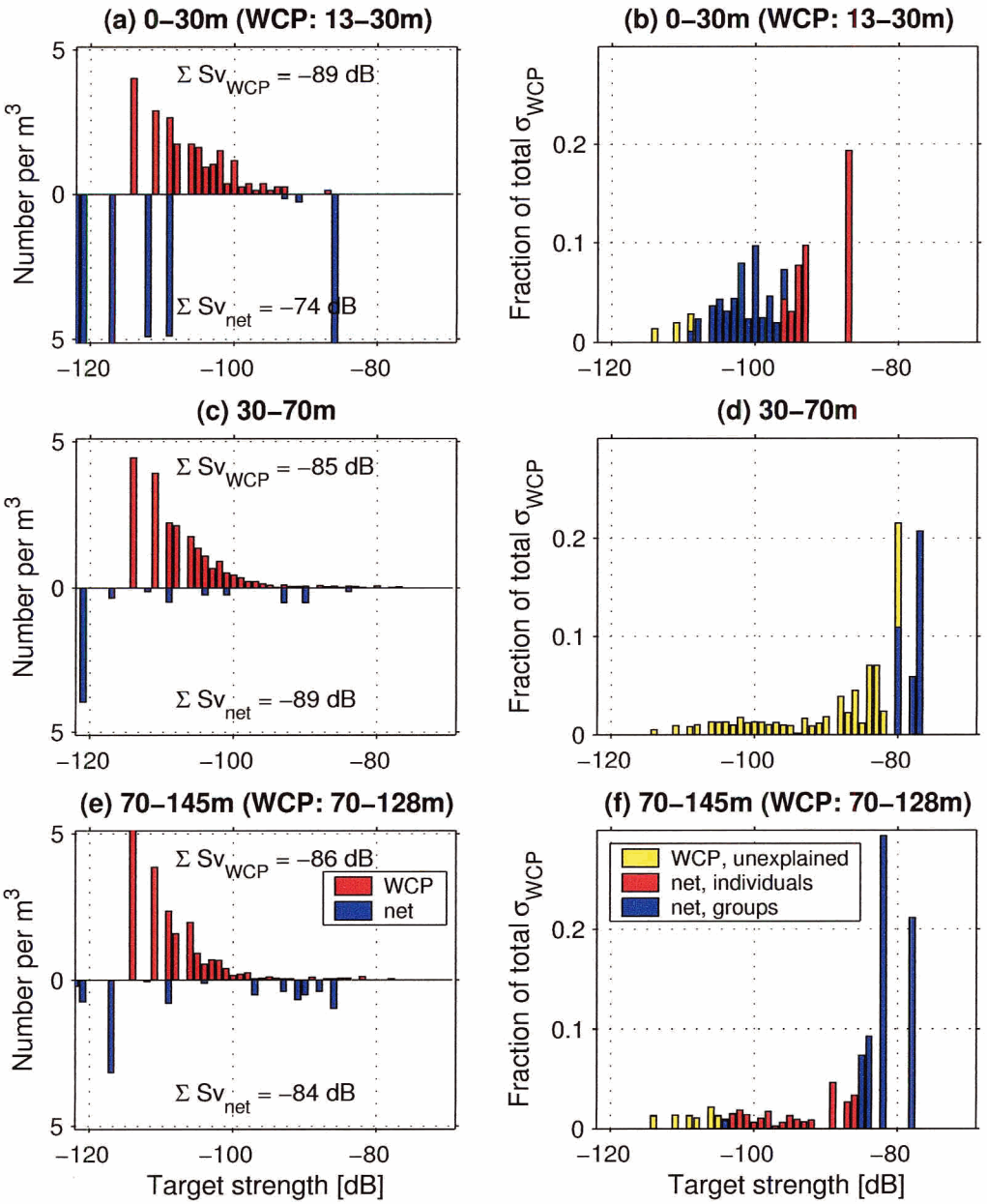

Figure 4.11: Histograms of target strength obtained from three sets of net data (a,c,e) and results of matching the net histograms to those for the WCP data (b,d,f). Net data were collected from station KN06 on June 20, 2001 (b,c,e in Table 4.1). WCP data are from June 22, using samples from 3 m range in front of the transducer. Left-hand panels: histograms of target strength for the nets and the WCP sections. Right-hand panels: WCP backscatter, accounted for as individual organisms and/or groups of organisms collected in the nets (details discussed in the text).

Station	*Label*	*Histogram comparison*		
		*% of σ_{wcp} explained**	*% of σ_{wcp} from individuals**	*% of WCP targets from individuals**
KN05	(a)(1)	100 (91)	60 (48)	21 (9)
	(a)(2)	101 (96)	74 (37)	100 (5)
KN06	(b)	102 (95)	100 (67)	100 (4)
	(c)	33 (33)	0 (0)	0 (0)
	(g)	46 (46)	0 (0)	0 (0)
	(d)	100 (100)	7 (6)	27 (13)
	(e)	90 (90)	6 (6)	15 (15)
	(f)	93 (93)	1 (1)	11 (11)
KN04	(h)	100 (68)	93 (50)	28 (3)
	(i)	100 (46)	22 (0)	21 (0)

Table 4.2: Comparison between WCP acoustic data and net predictions of the frequency distribution of scattering volume. Labels in the second columns refer to Fig. 4.10/Table 4.1. The last three columns show the portion of the total WCP backscatter that could be accounted for from the net data (matching target-by-target), and the portion that could be explained as returns from individual organisms (in terms of total backscatter (red bars in Fig. 4.11) and numbers of WCP returns). (*results obtained by using only the fluid-like taxa are shown in parentheses)

in Fig. 4.11(b), resulting mainly from a lesser abundance of amphipods than in similar casts, resulted in a poor accounting of the WCP data. As with these two examples, it was sometimes possible to associate disparities between the net and WCP data with variations in the abundance of a single species. For example, if the comparison shown in Fig. 4.11(b) is carried out with the net cast taken on the other side of the sill on the same day (which contained a larger number of amphipods), twice as much of the WCP backscatter can be accounted for.

Despite these limitations, some trends were repeatedly observed over multiple combinations of net and WCP data. In terms of the total portion of the WCP data explained by the net data, it was found that the frequency distribution of target strengths predicted from the nets could very often be used to account for all, or almost all, of the backscatter observed by the WCP (Table 4.2), particularly in cases where the average scattering volumes were not too dissimilar. While there was little or no benefit in pairing net and WCP data from the same side of the sill, WCP sections tended to be better explained by net tows from reasonably similar depth ranges (e.g., deep net tows could not explain near-surface WCP data).

The relative contributions from single organisms (red bars in Fig. 4.11(b,d,f)) and groups of organisms (blue bars) also varied a great deal over the pairings considered. However, where the the net did not significantly over- or under-estimate average WCP returns, a large proportion of WCP samples were accounted for as the sum of returns from more than one organism (Fig. 4.11, Table 4.2). Many histograms of WCP data included returns stronger than any predicted from the net data (e.g., Fig. 4.11(c,e)). Mid-water WCP sections commonly included targets as strong as -77 dB; while a few such targets could be due to particularly large net organisms at broadside incidence, all WCP targets over -86 dB must be explained as groups under the more likely assumption of random orientation.

An alternative explanation is that the nets under-sample large, strongly-scattering organisms as a result of active avoidance by these animals; if this were the case, it may be possible to explain all moderate-strong WCP returns as individual organisms. However, if this avoidance is "corrected" by adding such scatterers into the calculations for the net predictions of scattering volume, the resulting predictions are consistently too large; i.e., the average scattering volumes become much higher than those observed by the WCP. Thus, this explanation seems unlikely, and it seems more plausible that these target strengths were due to small groups of moderately-sized organisms. The numbers of organisms required to account for individual WCP returns, typically 2-8 individuals, are not unrealistic in an insonified volume approximately 21.7 cm in length by 50 cm in diameter, although they require a considerable local increase in abundance; the average number densities of most organisms over -100 dB would yield less than 0.24 individuals in the same volume. These increased densities must be explained either as scattering layers (e.g., (e) in Fig. 4.10) or as smaller, localized aggregations.

For target strengths up to -86 dB, the WCP data may be explained as a combination of individual organisms and groups; individuals could account for a significant portion of the total backscatter, even though they generally represented a relatively small proportion of the total number of WCP samples (Table 4.2). The split between individuals and groups at these target strengths varied considerably, and depended on the particular pairs of WCP and net data being compared. Additional features of the acoustic data must be used to characterize such WCP returns.

4.3 Small-Scale Distribution of Acoustic Backscatter

4.3.1 Properties of Strong Acoustic Targets

Further information may be obtained by considering complete images of short sections of WCP data, such as those shown in Fig. 4.12. As discussed in Section 3.1.3, these images are made up of a series of slanted pings (slanted because of the downward pitch of the instrument in these figures), separated in time by the ping interval of 1 s, and each consisting of a "row" of samples collected along the ping at 23.3 kHz. Each ping begins slightly deeper (in this case) and further along the transect than the previous one, due to the motion of the vehicle; note that while the angle of descent and the pitch are often similar, during a steep descent the vehicle pitch may be slightly shallower (e.g., Fig. 4.12(b)). The motion and attitude of the vehicle, as recorded by TOMI electronics, are used to plot each the samples in terms of depth and distance along the transect. Thus, information may be gathered on the horizontal extent of acoustic features by looking horizontally across the "ribbons" of acoustic data in Fig. 4.12. In addition, because the beam width for most ranges is greater than the vertical separation between pings, a single volume of water will be sampled a number of times before it exits the beam. As a result, a single target will appear in a number of pings; such objects appear as vertically "smeared" returns in the WCP images (e.g., the strong red target at 15 m distance in Fig. 4.12(b)), yielding some information on the persistence of structures as well.

Although such images of WCP data consisted mostly of abundant weaker returns (i.e., $Sv \lesssim -90\,\mathrm{dB}$), the average scattering volumes were strongly influenced by rare moderate to strong returns. Some of these were observed in only one ping, and in some cases (e.g., far range, high ϵ and dT/dx) cannot conclusively be associated with zooplankton. However, most images contained at least a few strong, clearly defined, discrete targets, which could be recognized at approximately the same location over several pings as the vehicle moved along its path (e.g., yellow and red vertical "streaks" in Fig. 4.12). Depending on the region and the range at which targets were first detected, the depth interval between the first and last returns varied from approximately 20 cm to over 2 m, and was generally at least slightly less than predicted from the beam width, rate of ascent/descent, and vehicle speed. In addition, while

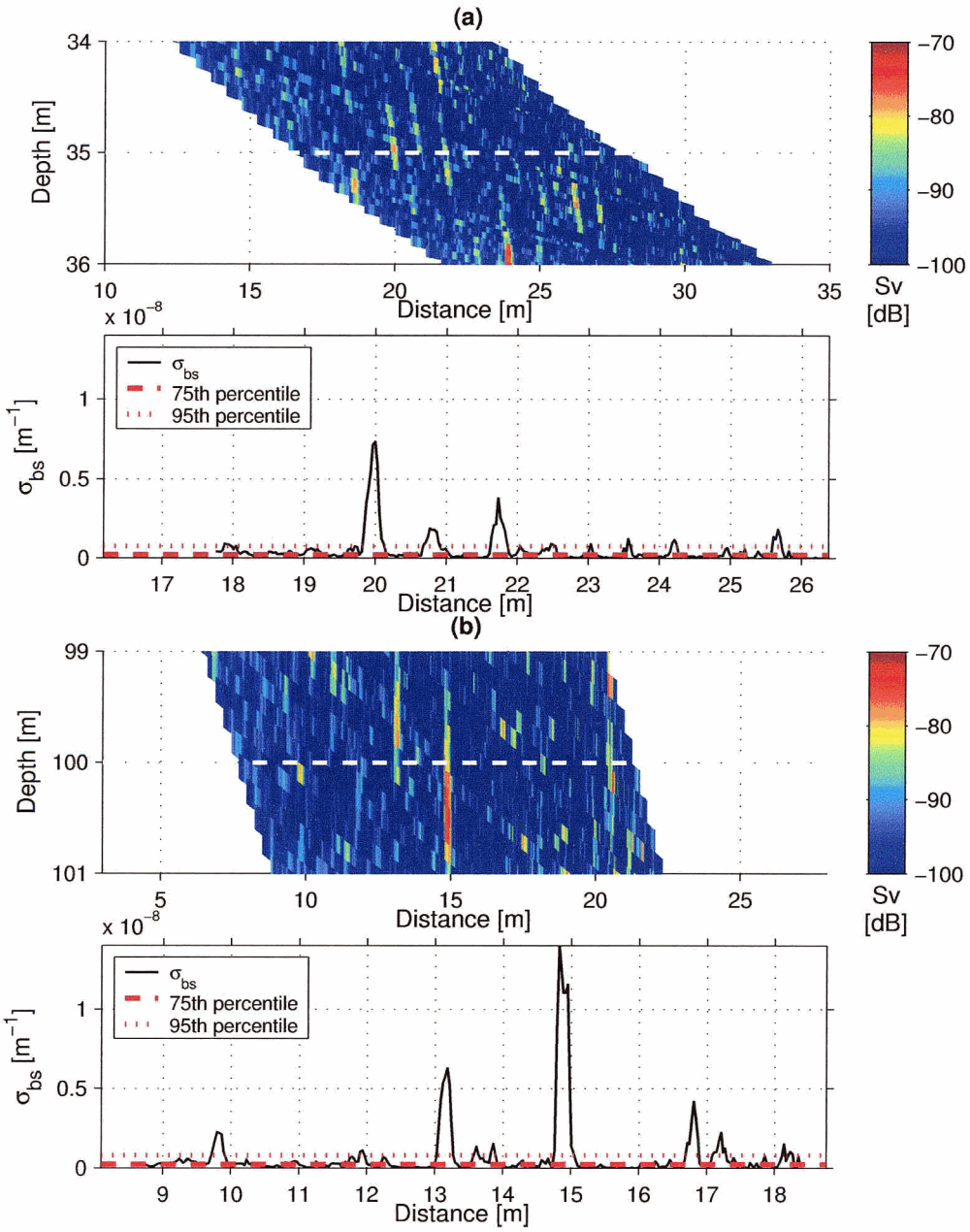

Figure 4.12: Extraction of spatial series from WCP data collected between 9:00 and 9:15 on June 22, 2001. Spatial series extracted along the dashed lines in the top panels of (a) and (b) are shown in the bottom panels. Note that the the first (closest range) 30 samples (90 cm) of each WCP ping are not shown in the top panels of (a) and (b) (transducer ringing). Average scattering volume was -92 dB in each case.

most of these targets were weaker and narrower in the first and last pings in which they were observed, consistent with entering and exiting the acoustic beam, it was not uncommon for targets to break up into narrower objects or otherwise abruptly disappear. If the target is assumed to represent an individual organism, such abrupt disappearances may be explained by rapid swimming out of the acoustic beam; if aggregations are involved, then the number of pings over which the scatterer was observed reflects the length of time during which the organisms remained aggregated (starting from the point in time when they entered the beam or were seen to come together), and we may talk about the relative persistence of the aggregation.

Targets in the WCP images are readily identified as strong, distinct peaks in spatial series of backscattering cross-section (lower panels in Fig. 4.12). Even moderate peaks (i.e., cyans and greens in Fig. 4.12) were stronger than 95% of the surrounding samples, and could be clearly distinguished from the surrounding spatial series at the 75^{th} percentile. These peaks were generally irregularly shaped, and appeared to be the sum of two or more narrower spikes (Fig. 4.12). Widths (measured at the 75^{th} percentile of σ_{bs}) were typically between 35 and 50 cm, although targets up to one metre in width occasionally occurred. Taking into account the pulse length, this points to aggregations around 13-28 cm in size. While the width, shape, and strength of the targets varied from ping to ping, the targets were generally recognizable until they disappeared from the image. In contrast, those targets which were only observed in a single ping often occurred as a single peak, narrower than the pulse length.

The number of strong, persistent targets varied considerably from image to image. In typical sections from quiescent regions (e.g., Fig. 4.10), spatial series extracted from 1-15 m range in front of the transducer (chosen to avoid higher noise levels at far range) typically contained 2-6 peaks at or above the 95^{th} percentile for σ_{bs}, with spacings from tens of centimetres to a few metres. Of these, 1-4 generally persisted over at least 0.5 m of change in TOMI's depth (a total insonified volume of approximately $10\,\text{m}^3$). The frequency of occurrence of persistent targets was somewhat lower than might be predicted from the nets ($0.1 - 6\ \text{m}^{-3}$ for organisms with TS ≥ -90 dB for all nets from Knight Inlet); this is consistent with the suggestion in Section 4.2.2 that organisms may often occur in small groups.

4.3.2 Variability in the Spatial Distribution of Scattering Volume

The distribution of backscatter within WCP images varied considerably from region to region, reflecting changing zooplankton number densities, sizes, and distributions (Table 4.3). For instance, shallower sections were generally characterized by larger numbers of weaker (cyan) targets, most of which were narrow (near the pulse length) and persisted for less than a few pings (Fig. 4.12(a)). Wider, stronger, more persistent targets were present against this "background", but still persisted over a shorter time and varied more from ping to ping than deeper targets. Deeper sections had less "background" scatter and larger numbers of very strong targets, which persisted over a greater change in TOMI's depth and which had greater maximum target strengths than returns from shallower sections (Fig. 4.12(b)). While the average widths of persistent targets did not appear to change systematically with depth, the shapes of deeper targets tended to be simpler, more often consisting of only two smaller peaks. These changes with depth often coincided with vertical distributions of backscatter observed with the ship-mounted echosounder; e.g., the WCP began sampling greater numbers of discrete, persistent targets as TOMI entered the scattering layer at approximately 45 m in Fig. 4.10.

Although dense acoustic scattering layers (e.g., Fig. 4.7) were not often sampled near the sill, the few sections of WCP data from such regions reflected the elevated number densities of medium-sized zooplankton responsible for the existence of these acoustic features (Fig. 4.13). Both average and maximum scattering volumes were

Dissipation rate	*Depth*	*Number density*	*Extent of aggregation*	*Aggregation persistence*	*Example of WCP data*
low	shallower	average	moderate	moderate	Fig. 4.12(a)
low	deeper	average	high	high	Fig. 4.12(b)
low	moderate	high	moderate	moderate	Fig. 4.13
high	shallower	average	low	low	Fig. 4.14(b)
high	deeper	average	moderate	low	Fig. 4.14(b)

Table 4.3: Summary of the small-scale zooplankton distributions observed around the sill of Knight Inlet in June, 2001. Extent of aggregation summarizes how much of the acoustic scatter in WCP images occurred as persistent targets vs. as "background" scatter, and the ping-to-ping variability in the targets; persistence refers to the relative number of pings over which targets were recognizable.

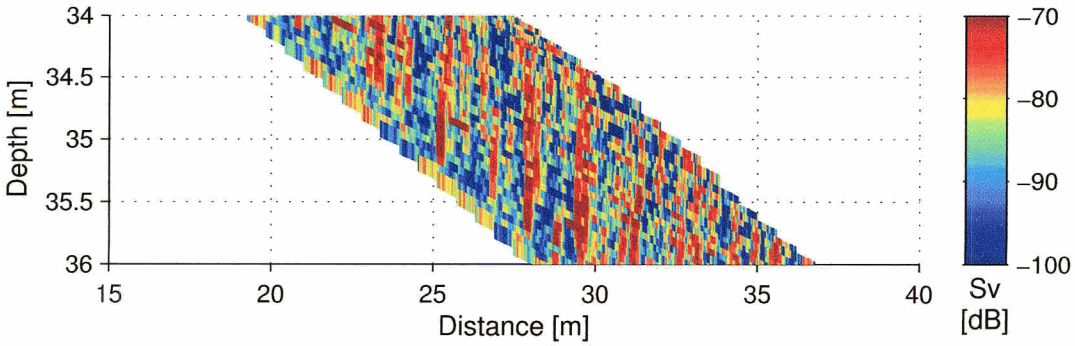

Figure 4.13: WCP data collected from a strong scattering layer east of KN07 (15:35, June 21). Average scattering volume was -78 dB. The corresponding ship-mounted echosounder data are shown in Fig. 4.7(a). Note that the the first 30 samples (90 cm) of each WCP ping are not shown (transducer ringing).

much higher within the layers (e.g., target strengths up to -74 dB in Fig. 4.13). While particularly strong targets could still be picked out, such images lacked the weak "background" typically observed. Closer packing of returns led to much wider targets (approaching one metre), whose shape and width varied more widely from ping to ping, and which often broke into smaller targets before exiting the acoustic beam (Fig. 4.13).

The appearance of WCP images also changed with varying levels of turbulence. The amount of useful WCP data collected from highly turbulent regions (i.e., $\epsilon \simeq 10^{-6}\,\mathrm{W\,kg^{-1}}$) was limited, due to the short duration of such conditions (Fig. 4.3) and the need to accommodate other sampling objectives during peak flows. Furthermore, the measurements may suffer from interference due to bubbles and turbulent microstructure. Despite these effects, however, persistent targets were observed at dissipation rates on the order of 10^{-6} W kg^{-1} (e.g., Fig. 4.14). Images from such regions tended to be "noisy", with many weaker, short-lived targets; compared to strong targets observed in quiescent regions, even reasonably persistent returns were observed for a relatively small number of pings (Fig. 4.14). Although the shapes and strengths of persistent returns were similar overall to those at lower dissipation rates, the widths were often less, closer to the pulse length. In addition, the shape,

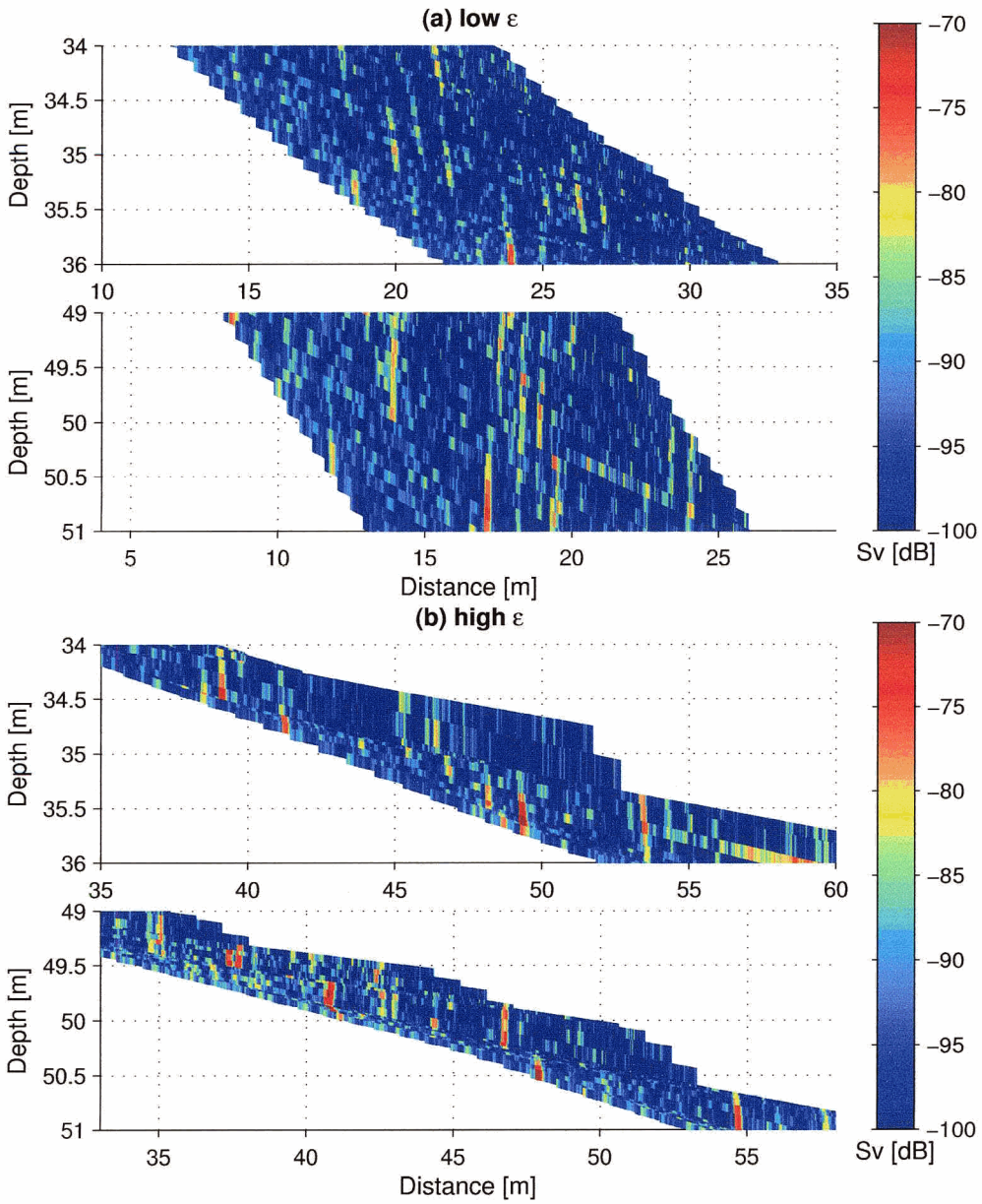

Figure 4.14: WCP data collected near the sill of Knight Inlet on June 22, 2001, shortly after slack tide (a, 9:05 PDT) and near the end of a large ebb (b, 8:10 PDT). Note that the the first 30 samples (90 cm) of each WCP ping are not shown (transducer ringing).(a) 35m: $\overline{\epsilon} = 1.3 \times 10^{-7}$ W kg^{-1}, $\overline{Sv} = -92$ dB; 50 m: $\overline{\epsilon} = 4.4 \times 10^{-9}$ W kg^{-1}, $\overline{Sv} = -92$ dB. (b) 35 m: $\overline{\epsilon} = 1.4 \times 10^{-6}$ W kg^{-1}, $\overline{Sv} = -88$ dB; 50 m: $\overline{\epsilon} = 9.7 \times 10^{-7}$ W kg^{-1}, $\overline{Sv} = -87$ dB.

width, and horizontal location varied more from ping to ping at higher dissipation rates. While these effects were observed at all depths, they were most pronounced for shallower sections (Fig. 4.14, Table 4.3).

These examples illustrate some of the variability seen in zooplankton distributions around the sill, as summarized in Table 4.3. If the strong targets shown in Figs. 4.12-4.14 are taken to be aggregations, then these were most clearly defined and most persistent in deeper regions (characterized by larger organisms) with low turbulence levels and moderate zooplankton concentrations. By comparison, shallower regions had more non-persistent returns and less stable aggregations, and the wide, strongly scattering aggregations observed in a dense scattering layer were considerably more variable from ping to ping. Similarly, comparing acoustic data collected from similar regions at low vs. high dissipation rates, aggregations were more variable and shorter-lived when turbulent mixing was more intense.

Chapter 5

Discussion

5.1 Flow Over the Sill and Large-Scale Plankton Distributions

The flow over the sill of Knight Inlet sets the stage for the physical-biological interactions which occur there. As observed by Farmer and Armi (1999), tidal forcing in this region produces regularly varying current speeds and turbulent intensities. During this survey, flow speeds increased from near-slack to over 1 ms^{-1} at mid-tide, while dissipation rates increased by over five orders of magnitude. Interaction with surface stratification and bottom topography produced particularly high shear near the surface and in the lee of the sill, where lee waves were observed during larger ebb tides (discussed in detail by Farmer and Armi (1999)). As a result, organisms near the sill may experience considerable changes in local velocity and shear over time scales of hours and spatial scales of tens of metres or less. Non-motile organisms are advected by the flow, modifying their horizontal and vertical distributions; this was illustrated by measurements of the phytoplankton, which were dispersed over a greater depth range during peak flows. However, this effect was confined to a brief period near mid-tide, and on average phytoplankton around the sill were concentrated in the well-lit near-surface region.

Similarly, tidal flows appeared to modify overall zooplankton distributions only modestly. Larger organisms (amphipods and euphausiids) were able to form persistent scattering layers, similar to those further away from the sill, during most of the tidal cycle, and carried out normal daily vertical migrations; these layers have been

observed in other surveys of this area (Trevorrow 2001, 2002) and appear to be a recurring, possibly permanent, feature of the Inlet. Although the downstream layers were disrupted during peak flows, likely due to turbulent mixing and/or swimming behaviour, these effects only lasted while flow speeds were highest. However, changes in feeding or predation during such times may be large enough to significantly impact overall growth and recruitment. For example, planktivorous fish may take advantage of zooplankton being moved up against the sill, resulting in increased predation mortality (Trevorrow 2001, Mackas et al. 2002); this appeared to be the case during this survey, based on the presence of strong scatterers, believed to be fish, on the upstream edge of the sill. In addition, regular variations in velocity and shear on scales relevant to individual zooplankters may influence feeding success, growth, and reproductive ability (see Section 2.1), potentially affecting population growth on the whole, and motivating the investigation of smaller-scale patterns.

5.2 Ground-Truthing the Acoustic Data

Collection of zooplankton samples using vertical net hauls made it possible to ground-truth the WCP data, providing a basis for further interpretation of the backscatter measurements. Despite the variety of zooplankton species captured in the nets (Appendix A), it was possible to predict the average backscatter using only two models (for randomly oriented fluid cylinders and elastic-shelled spheres, as described by Stanton et al. (1994)) and four taxonomic groups (copepods, amphipods, euphausiids, and pteropods). This simplification increased the overall robustness of the ground-truthing process, as the models involved are relatively simple and well-established in the field (e.g., work by Wiebe et al. (1997)). The modelling process highlighted the importance of contributions from moderate to large organisms to average backscatter, despite their relatively low abundance; thus, as observed by Wiebe et al. (1997), acoustic measurements may tend to reflect size distributions more than total biomass of organisms present. This was particularly true in regions where pteropods were abundant, due to the strong backscatter from their aragonite shells.

Applying these models to the number densities and size distributions of zooplankton captured in the nets, it was possible to approximately account for the acoustic returns observed with the WCP, suggesting that the WCP was able to provide a reasonable measure of the zooplankton community. Not surprisingly, the comparisons

were most successful when sections with similar average scattering volumes (suggesting similar zooplankton biomass) were compared. In addition, while location and collection day did not appear to significantly impact the ability of a net to explain a section of WCP data, comparisons were more successful when data from similar depth ranges were used. This may be expected given the depth-dependence of zooplankton size distributions, demonstrated by the net data, and the central role of an organism's size in determining its backscattering cross-section. While it was unclear whether or not such vertical variations were a significant source of error when comparing net and WCP data collected over slightly different depth ranges during this survey, identical ranges would clearly be desirable.

Although it was possible to roughly compare the net and WCP data, both data sets were highly variable, preventing direct comparisons between these necessarily non-simultaneous sets of measurements. Assuming that the overall community structure did not change significantly from day to day during the survey, a reasonable assumption considering the time scales of the processes that could produce such change (Mackas et al. 1985), this variability likely reflects sampling of highly heterogeneous, or patchy, zooplankton distributions; in fact, such patchiness at scales of metres and hours has been well-documented (e.g., reviews by Mackas et al. (1985) and Folt and Burns (1999)).

In addition to providing an independent estimate of acoustic backscatter from zooplankton, the net data established what species and sizes of organisms were present, and so available to form the distributions that were observed with the WCP. For example, strong returns in the acoustic data could only rarely be associated with individual organisms in the nets (either amphipods or euphausiids); generally, comparison between predicted and observed distributions of target strengths pointed to small aggregations of moderate to large copepods, amphipods, and/or euphausiids. This interpretation may not be realistic if larger organisms regularly avoided the nets, and so were under-represented in the samples; however, this should result in the nets consistently under-estimating the backscatter measured by the WCP, and this did not appear to be the case. Ideally, measurements of undisturbed micro-scale zooplankton distributions and species composition would be made very nearly simultaneously, allowing for detailed interpretation of the species involved in the aggregations. However, in the absence of such simultaneous data, which often requires elaborate and expensive equipment to collect, non-simultaneous measurements such as those col-

lected on this survey allow for a general description of the micro-scale distributions in terms of the species found in the region.

5.3 Small-Scale Zooplankton Distributions

When comparing the WCP data with the nets, which measure numbers of organisms per volume of water filtered, it is convenient to deal with the acoustic data as a series of samples, each representing the total backscattering cross-section within an insonified volume. In contrast, discussion of the distributions of organisms requires moving from this sampling entity to an acoustic entity, i.e. a discrete return or target, which in turn represents a biological unit, either an individual or a group of individuals. This involves considering two-dimensional images of short sections of WCP data (e.g., Figs. 4.12-4.14), in which repeated sampling of undisturbed targets yields information on both their horizontal extent (along-ping) and their persistence (ping-to-ping).

Such images are dominated numerically by relatively weak returns (Sv less than approximately -90 dB) that are observed for only one ping. Given the overall agreement between average scattering volumes measured by the WCP and those predicted from the nets, it is likely that most such returns correspond to real scatterers; for example, a 3.65 mm copepod would have a scattering volume of approximately -90 dB at 5 m range, and could escape out of the beam in the time interval between two pings (Haury et al. 1980). However, little can be said about the properties of such objects based on a single observation, which does not provide enough information to distinguish between a small organism, a large organism off the transducer axis, and electronic or environmental noise. Not surprisingly, such returns are more common near the surface, where the zooplankton community is populated by smaller organisms, which may be nearer the detection limit of the echosounder.

Although such weak targets represent the most common type of return, the largest contribution to total backscatter comes from discrete, persistent targets, i.e. strong peaks in the returned signal which have a clear beginning and end, and which can be recognized at the same location over at least a few pings (e.g., Figs. 4.12 and 5.1). While this definition is too subjective to be used to identify and count all the persistent targets in an image (e.g., it may often be difficult to visually identify a weaker target), it is adequate to consider examples of targets from different regions or stages of the tide. It also ensures that only real objects are discussed, even at

higher levels of turbulence, where discreteness can be used as a criterion for distinguishing zooplankton from turbulent backscatter (Ross 2003, Ross and Lueck 2004). Additionally, these moderate-strong, persistent returns include a biologically interesting group of organisms, namely moderate-sized animals (a few millimetres or more in length) which are likely to have some control over their positions.

5.3.1 Distributions at Low Turbulence

Most of the net and WCP data used in this work were collected at the relatively low turbulent intensities (ϵ on the order of 10^{-8} to 10^{-7} W kg^{-1}) which were typical of the greater part of the tidal cycle. As discussed in Section 5.1, the vertical distributions at these times were similar to those observed away from the sill, and may be thought of as relatively "undisturbed".

Zooplankton Aggregations

Despite the relatively low number densities (i.e., relatively large average separations) of medium-sized organisms captured in the nets (Fig. 4.6), most of the persistent targets that were observed throughout the area around the sill appeared to represent aggregations, i.e. groups of two or more individuals spaced too close together to be resolved by the echosounder. While this applied to most discrete, persistent, moderately strong ($Sv \gtrsim -90$ dB) targets, it was particularly true of stronger returns (approaching -80 dB), almost all of which appeared to be clusters of organisms. This conclusion was supported both by the nets, which captured too few large organisms ($TS \geq -86$ dB) to account for all moderate-strong WCP returns, and by the widths and shapes of the targets themselves. These pervasive aggregations were typically between approximately 10 and 30 cm in width, making these structures among the smallest described in the literature; Davis et al. (1992) provide perhaps the only other definite observation of patchiness at scales of tens of centimetres, although other observations have been made at scales around 1 m (Currie et al. 1998, Gallager et al. 1996, 2004). However, because relatively few instruments currently exist that can measure distributions at such scales, it is unclear whether or not zooplankton in Knight Inlet were actually aggregated at smaller scales than in other regions, and if so, why this might be the case.

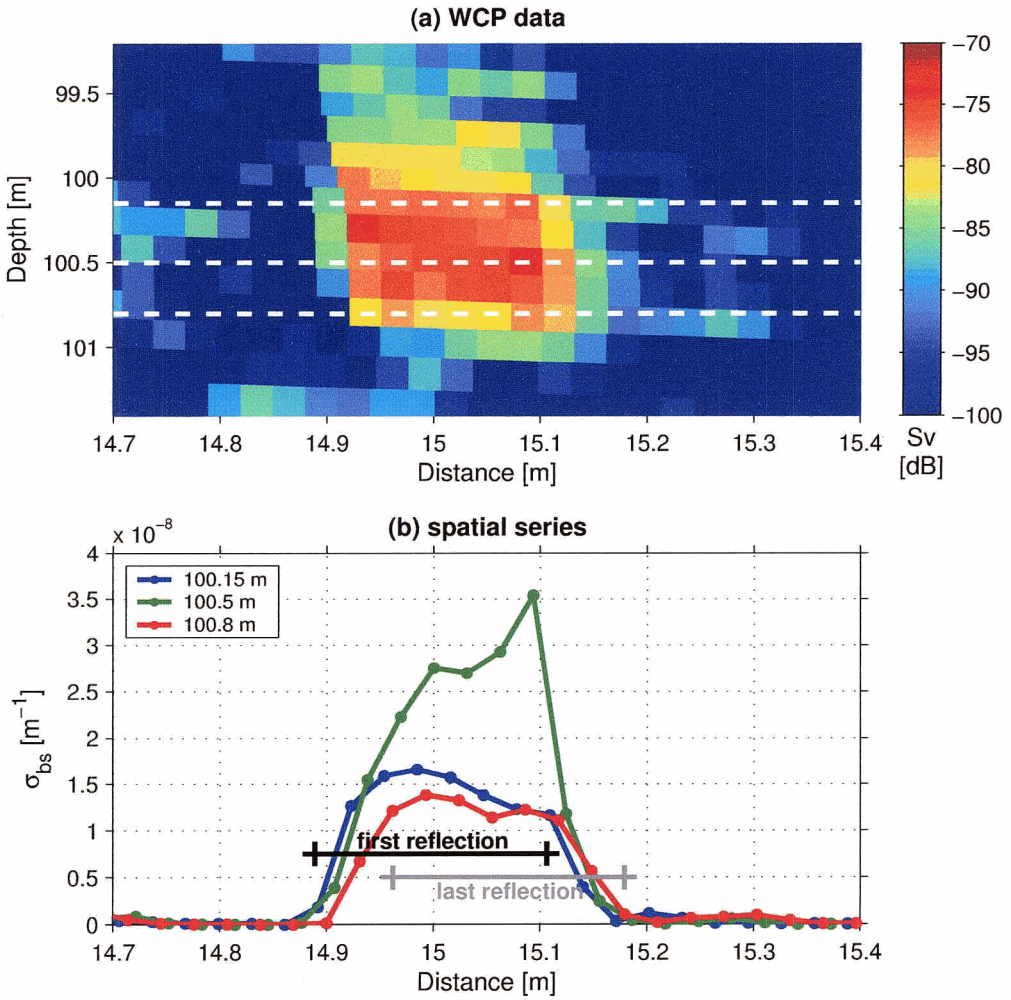

Figure 5.1: Acoustic returns from a single target, taken from the region shown in Fig. 4.12(b). Spatial series extracted along the dashed lines in (a) are shown in (b), along with the approximate horizontal locations of the first and last reflections from the target. For a single ping, the return from the target starts when the first 300 μsec pulse, reflected from the organism at shortest range (black bar), arrives at the transducer, and ends at the trailing edge of the pulse reflected by the most distant organism in the aggregation (gray bar). The real width of the aggregation is the difference between the ending points of the first and last reflections.

Aggregations exhibited a level of ping-to-ping variability, perhaps due to the motions of the component organisms; the width, shape, and strength of targets generally underwent small random variations from ping to ping, and aggregations sometimes separated before leaving the beam (e.g., Fig. 5.1). These variations were greater in near-surface targets, whose smaller members were unable or unwilling to form aggregations as tight and as persistent as those formed by the larger organisms found at greater depths. The stability of aggregations was also reduced in scattering layers; aggregations within these layers formed and broke apart over shorter time scales than in regions of lower number density, perhaps as a result of increased interactions between organisms. Interestingly, Greene et al. (1992) noted decreased average patchiness in intense daytime scattering layers compared with the lower density layers they observed at night, although it is unclear whether or not these observations are related to those discussed here.

Although densities within the aggregations cannot be determined directly from the data collected, some rough estimates may be made from the target shapes and net data. For example, considering the target shown in Fig. 5.1:

1. Because the target is wider than the 300 μsec (21.7 cm) pulse length, it must be the sum of reflections from at least two scatterers, forming the leading and trailing edges of the target (Fig. 5.1(b)); for example, two juvenile euphausiids ($\approx$ 10 mm) at broadside incidence would reflect strongly enough to explain the return. Similarly, any aggregation with an apparent width greater than the pulse length by a factor of 1 to 2$\times$ (i.e., 21.7-43.4 cm) must be made up of at least two organisms, and targets wider than 43.4 cm must include at least three. Note that these dimensions refer to the apparent width of the target in the images; the actual patch width is shorter by the pulse length of 21.7 cm (Section 3.1.3).

2. If zooplankton are randomly oriented, then organisms at broadside incidence can only occasionally be used to explain targets. In this case, comparing the frequency distribution of target strengths measured with the WCP to that predicted from the nets suggests that each of the two or more strong returns making up the target in Fig. 5.1 is itself likely to be the sum of reflections from up to 8 organisms; thus, based on the argument in Point #1, the target in Fig. 5.1 could include as many as 16 organisms. The shape of the return may be misleading

in this case, as organisms may be spaced more closely than the resolution of the echosounder.

These estimates may also be used to make a rough guess of the nearest-neighbour distances within the aggregations. For example, 2-16 organisms in a patch 10 cm in width (apparent target width of 31.7 cm, in the middle of the range in Point #1) would imply average separations ranging anywhere from 0.7 to 10 cm, considerably closer than would be expected from the number densities measured by the nets. By comparison, the spacing between aggregations was relatively large, usually around 1 m or more. The close spacing within patches, and the disparity between within-patch and between-patch scales, argue against the aggregations occurring by chance, as a random distribution of organisms would imply a Poisson distribution of separations; instead, organisms in Knight Inlet tended to be spaced either rather close together or rather far apart, but not, generally, somewhere in between.

Causes of Patchiness?

At the low turbulent velocities observed near slack tide, active swimming by zooplankton is the only process acting on temporal and spatial scales short enough to produce the small aggregations we observed (Mackas et al. 1985, Folt and Burns 1999). While this work did not address the causes of zooplankton patchiness, some processes which may be plausible in Knight Inlet include the following:

- Feeding: Relatively long diatom chains were observed in the nets, and zooplankton may aggregate as a result of feeding on these clumped cells or within larger phytoplankton patches. Many of the taxonomic groups observed in Knight Inlet are able to respond to increased food concentrations by changing their swimming patterns (De Robertis 2002). However, this explanation depends on there being similarly small scales of patchiness in the phytoplankton, which may or may not be the case.

- Mating: Zooplankton have evolved elaborate behaviours to find and track mates, and may interact for tens of seconds in the process (Howlett 1998, Strickler 1998, Yen et al. 1998). Such mating aggregations were believed to be the cause of the micropatches observed by Davis et al. (1992). A number

of Knight Inlet species reproduce during the summer, including the large amphipod *Primno abyssalis* (Yamada et al. 2002) and the euphausiid *Euphausia pacifica* (Kathman et al. 1986, Mackas et al. 1997); in particular, the presence of euphausiid eggs in the nets makes this explanation plausible for the adult euphausiids found at greater depths.

- Social: Some species, particularly euphausiids, are commonly observed to form social aggregations, for reasons which may include feeding efficiency and predator avoidance (Greene et al. 1992, Ritz 2000). Although *E. pacifica* does not always form aggregations, particularly where deep vertical migration is available as a means of predator avoidance (De Robertis 2002), predation pressure by planktivorous fish (e.g., Mackas et al. 2002) could favour such behaviour in the relatively shallow region around the sill of Knight Inlet.

Naturally, no one factor is likely to account for all aggregations, and the relative roles of these and other forces will depend on the species involved and their behaviours. For example, the second two processes require that zooplankton within the aggregations be aware of one other. Comparing the rough estimate of nearest-neighbour distances made above (0.7-10 cm) to typical zooplankton perceptive distances of 2-4 body lengths (e.g., 1-2 cm for a 5 mm organism, Haury and Yamazaki (1995)), organisms are only likely to directly perceive one another in the densest patches. Nonetheless, the use of cues such as odour trails may extend this distance at low turbulent intensities, particularly in the case of mating (Yen et al. 1998).

5.3.2 Distributions at High Turbulence

Compared with the images described in the preceding section, WCP data from more turbulent regions ($\epsilon \gtrsim 10^{-6}$ W kg^{-1}) contained larger numbers of low- to moderate-intensity, non-persistent returns (Fig. 4.14); although this may suggest larger numbers of unaggregated organisms, increased environmental noise from temperature and salinity microstructure makes it difficult to determine whether or not this was actually the case. Persistent targets could be distinguished from the environmental noise, however, and as at lower dissipation rates, were generally associated with aggregations. While these aggregations remained common at elevated dissipation rates, they tended to be narrower, more changeable from ping to ping, and shorter-lived than

their low-turbulence counterparts, particularly in shallower regions. Two explanations are possible for these changes: turbulent mixing may actively dissipate aggregations, and/or some zooplankton species may be less inclined to form and maintain aggregations when mixing is more intense.

The role of turbulent mixing may be evaluated by considering the scales on which turbulent velocity fluctuations may affect zooplankton. The ranges of length and velocity scales produced by turbulent mixing are defined by the Ozmidov and Kolmogorov scales, which describe the largest and smallest eddies, respectively, in the cascade of turbulent kinetic energy (Section 2.1, Fig. 5.2(a)). Consistent with formation of aggregations by zooplankton swimming rather than turbulent stirring, the sizes and separations of zooplankton aggregations did not appear to be directly defined by these length scales. However, the magnitude of the relative velocities experienced by zooplankton over scales relevant to patch formation may determine whether or not zooplankton are able to maintain such aggregations. These relative velocities may be estimated from Eqn. 2.3, as illustrated in Fig. 5.2(b). At lower dissipation rates ($\epsilon \lesssim 10^{-7}$ W kg^{-1}), the relative velocities experienced on scales comparable to nearest-neighbour distances and patch sizes are less than the swimming speeds of most organisms, and aggregations are readily maintained, particularly for the larger organisms found at greater depths (Table 5.1). As dissipation rates increase, however, fewer and fewer organisms can resist local velocity fluctuations (Fig. 5.2(b)), and aggregations will break apart. Because of the intermittent nature of turbulence, it may still be possible for some organisms to form aggregations some of the time, but these will eventually be disrupted. The net result should be fewer and shorter-lived aggregations at higher dissipation rates; while not enough data was available from high-turbulence regions to test the first part of this statement, the second is consistent with our observations.

At smaller length scales, turbulent velocities are generally too low to directly modify zooplankton distributions (Fig. 5.2(b)), but the increased hydrodynamic disturbances experienced by the organisms may increase metabolism and affect interactions with prey, predators, and other members of the same species (Section 2.1). For example, increased velocity fluctuations may result in more frequent escape responses and/or changes in foraging behaviour (Costello et al. 1990), perhaps allowing zooplankton to deal more effectively with changing rates of encounter with prey and predators. Velocity fluctuations on the scale of body lengths may also reduce the

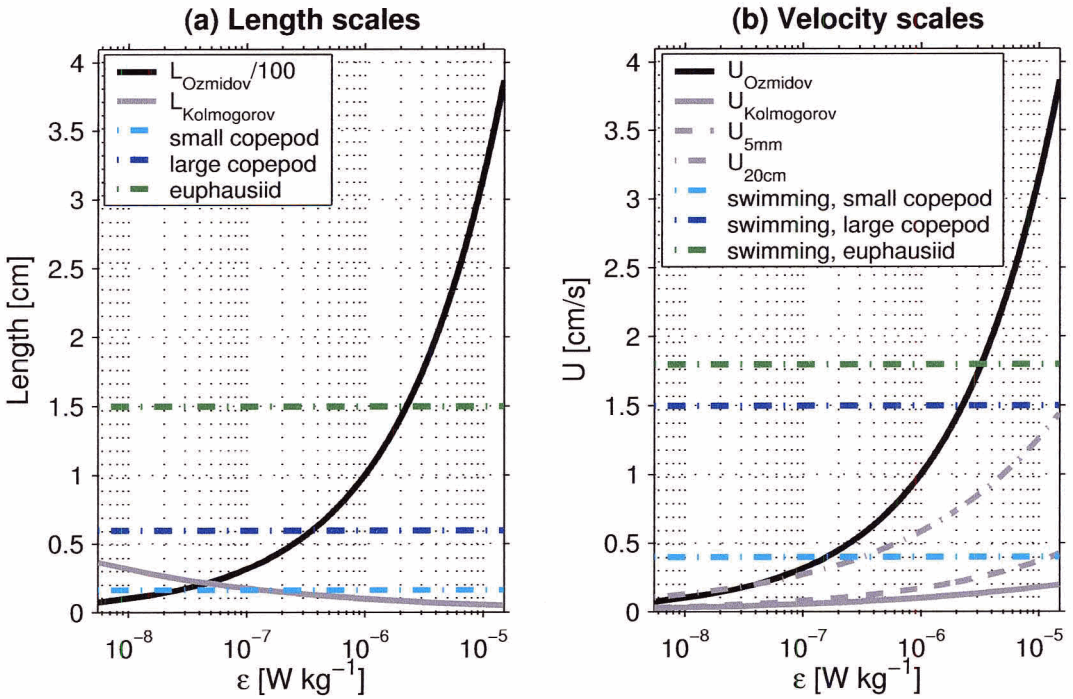

Figure 5.2: Comparison between length and velocity scales associated with turbulent eddies and with zooplankton swimming and patch formation. Approximate turbulent length and velocity scales are calculated from Eqns. 2.1-2.3, with $\nu = 1 \times 10^{-6}\,\mathrm{m^2 s^{-1}}$ and $N^2 = 1 \times 10^{-4}\,\mathrm{rad^2 sec^{-2}}$. Examples of zooplankton lengths and swimming speeds are shown for *Pseudocalanus minutus* (Buskey et al. 1987, length from Knight Inlet data), *Calanus finmarchicus* (Hardy and Bainbridge 1954, Haury et al. 1980), and *Euphausia pacifica* (De Robertis et al. 2003). Examples of turbulent velocity scales (accurate to within a constant of order one) are shown in (b) for the Kolmogorov and Ozmidov scales, as well as for scales similar to zooplankton body sizes ($\approx 5\,\mathrm{mm}$) and patch sizes ($\approx 20\,\mathrm{cm}$).

ability of zooplankton to perceive one another by chemical and hydrodynamic cues, which may be important if aggregations serve social or mating purposes. Thus, it is possible that the observed changes in distribution are a result of both physical and biological processes; further investigation would be required to determine the relative contributions of each.

Zooplankton distributions were only modified for a short portion of each tidal cycle, and the patterns described in Section 5.3.1 may be more indicative of "typical" conditions in Knight Inlet than those discussed here. However, because of the

Group	*Species*	*Swimming speed* [cm s^{-1}]	*Reference*
Amphipods	*Monoporeia affinis*	5	Lindström and Fortelius (2001)
Copepods	*Oithona davisae*	0.08	Yamazaki and Squires (1996)
	Acartia tonsa	0.25	Gallager et al. (2004)
	*Pseudocalanus minutus**	0.4	Buskey et al. (1987)
	*Metridia pacifica**	0.4	Yamazaki and Squires (1996)
	Euchaeta rimana	0.7	Yamazaki and Squires (1996)
	Calanus finmarchicus	0.15	Hardy and Bainbridge (1954)
Euphausiids	*Euphausia pacifica**	1.8	De Robertis et al. (2003)
	Euphausia superba	2.6	Ritz (2000)

Table 5.1: Typical swimming speeds of several zooplankton species. Species marked with an asterisk were captured in Knight Inlet; with the exception of *Monoporeia affinis*, all other organisms belong to genera that were observed in the Inlet.

relationship between small-scale distributions, turbulent mixing, and processes such as feeding, mating, and predator avoidance, such short-term changes could translate into longer-term effects on average growth, mortality, and reproduction, particularly if zooplankton tend to be retained near the sill for some time before being swept up or down the Inlet. While this survey did not attempt to assess the results of these processes, it is likely that aggregation, and the physical environment that modulates it, play an important role in the lives of zooplankton around the sill of Knight Inlet, and must be taken into consideration in ecological studies of this and similar environments.

Chapter 6

Conclusions and Future Work

In a series of tows conducted around the sill of Knight Inlet, British Columbia, simultaneous small-scale measurements were made of dissipation rates and zooplankton acoustic backscatter over a wide range of turbulent intensities. The acoustic data were interpreted spatially and combined with community data obtained from zooplankton net casts to yield information on small-scale zooplankton distributions. Zooplankton were shown to exist in stable aggregations on scales of tens of centimetres at all dissipation rates, although higher turbulent intensities reduced the persistence of these structures. The major conclusions from this study are summarized in the following points:

- Towed, forward-looking acoustics were shown to be an effective method for measuring undisturbed horizontal zooplankton distributions at scales down to a few centimetres. Measured scattering volumes compared well against known number densities and size distributions of organisms. Additionally, repeated sampling of a given volume of water, combined with simultaneously recorded motion data from the towed vehicle, provided information not only on the scales of zooplankton distributions, but also on the persistence of such patterns.

- Acoustic backscatter from zooplankton could be estimated from simple models based on fluid cylinders and elastic shells, using only the four dominant zooplankton taxa observed in the Inlet. Applying these models to the net data highlighted the importance of contributions from medium-sized organisms to average scattering volumes, making acoustic measurements sensitive not only to total biomass but also to local size distributions. The models were robust

enough to produce reasonable estimates of acoustic backscatter from the organisms found in the Inlet, providing a means of interpreting acoustic measurements of zooplankton distributions.

- Aggregations around 10-30 cm in horizontal extent, spaced on the order of one metre apart horizontally, appeared to be a pervasive feature of zooplankton distributions around the sill of Knight Inlet. These aggregations, among the smallest reported in the literature, are believed to represent non-random clusters of organisms formed as a result of swimming. While it is unclear what cues or behaviours were involved, nearest-neighbour distances in some patches may have been small enough for social interactions such as mating to occur.

- Aggregation properties varied with the sizes and species of organisms present, with deeper, larger organisms forming tighter, more stable clusters than shallower, smaller ones. However, an exception to this trend was observed in dense scattering layers, where moderately large organisms formed dynamic, short-lived aggregations.

- While aggregations continued to exist at higher turbulent intensities, particularly where larger organisms where involved, they were less stable under such conditions. Comparison of turbulent velocities with zooplankton swimming speeds suggests that aggregations may be disrupted at high turbulent intensities, as velocity fluctuations reach levels where they exceed zooplankton swimming abilities and/or possibly interfere with inter-organism communications. Such effects, combined with larger-scale modifications to distributions, have the potential to significantly impact zooplankton growth and reproduction.

The results of this survey also suggest a number of possibilities for future work:

- The ability to collect zooplankton data (abundance, species composition, and size distribution) over short depth intervals and simultaneously with the acoustic data would be valuable in determining what organisms are aggregating, and consequently what behaviours are likely to be involved. This would be particularly useful when sampling scattering layers.

- The use of a narrower pulse length would increase the effective resolution of the acoustic data, making the identification of aggregations clearer, and possibly

revealing further detail.

- More advanced image processing may be useful in separating not only strong targets, but also some of the more weakly scattering objects sampled over a few pings by the WCP. Such approaches may make it possible to more quantitatively describe target properties, and the biological patterns they represent.

- Detailed observations of zooplankton behaviour may rule out or support other theories for patch formation, such as mating or social aggregations. Video systems currently exist that are capable of this (e.g., the VPR (Davis et al. 1992) and OASIS (Jaffe et al. 1998)), although considerable care must be taken to avoid modifying the behaviour being observed (e.g., McGehee and Jaffe 1996).

- Collection of zooplankton distribution data from other parts of Knight Inlet and from other regions and times of year may reveal whether or not small-scale aggregations such as those we observed are a common feature of zooplankton distributions, and/or what types of conditions are required to produce them. For example, *Euphausia pacifica* is a dominant member of the zooplankton communities of many British Columbia fjords, and it would be interesting to compare the spatial distributions of this commerically important species in such locations with those observed in Knight Inlet.

Bibliography

Abraham, E. R. (1998). The generation of plankton patchiness by turbulent stirring. *Nature*, 291:577–580.

Anderson, V. C. (1950). Sound scattering from a fluid sphere. *Journal of the Acoustical Society of America*, 22:426–431.

Ashjian, C. J., Davis, C. S., Gallager, S. M., and Alatalo, P. (2001). Distribution of plankton, particles, and hydrographic features across Georges Bank described using the Video Plankton Recorder. *Deep-Sea Research II*, 48:245–282.

Ashjian, C. J., Davis, C. S., Gallager, S. M., and Alatalo, P. (2002). Escape behavior of planktonic copepods in response to hydrodynamic disturbances: high speed video analysis. *Marine Ecology Progress Series*, 235:135–146.

Benfield, M., Wiebe, P. H., Stanton, T. K., Davis, C. S., Gallager, S. M., and Greene, C. H. (1998). Estimating the spatial distributions of zooplankton biomass by combining Video Plankton Recorder and single-frequency acoustic data. *Deep-Sea Research II*, 45:1175–1199.

Benfield, M. C., Davis, C. S., Wiebe, . H., Gallager, S. M., Lough, R. G., and Copley, N. J. (1996). Video Plankton Recorder estimates of calanoid copepod, pteropod, and larvacean distributions from a stratified region of Georges Bank with comparative measurements from a MOCNESS sampler. *Deep-Sea Research II*, 43(7-8):1925–1945.

Buskey, E. J., Mann, C. G., and Swift, E. (1987). Photophobic responses of calanoid copepods: possible adaptive value. *Journal of Plankton Research*, 9:857–870.

Chu, D., Wiebe, P., and Copley, N. (2000). Inference of material properties of zooplankton from acoustic and resistivity measurements. *ICES Journal of Marine Science*, 57:1128–1142.

Costello, J. H., Strickler, J. R., Marrasé, C., Trager, G., and Zeller, R. (1990). Grazing in a turbulent environment: Behavioral response of a calanoid copepod, *Centropages hamatus*. *Proceedings of the National Academy of Science of the United States of America*, 87:1648–1652.

Currie, W. J. S., Claereboudt, M. R., and Roff, J. C. (1998). Gaps and patches in the ocean: a one-dimensional analysis of planktonic distributions. *Marine Ecology Progress Series*, 171:15–21.

Davis, C. S., Flierl, G. R., Wiebe, P. H., and Franks, P. J. S. (1991). Micropatchiness, turbulence and recruitment in plankton. *Journal of Marine Research*, 49:109–151.

Davis, C. S., Gallager, S. M., and Solow, A. R. (1992). Microaggregations of oceanic plankton observed by towed video microscopy. *Science*, 257:230–232.

De Robertis, A. (2002). Small-scale distribution of the euphausiid *Euphausia pacifica* and overlap with planktivorous fishes. *Journal of Plankton Research*, 24(11):1207–1220.

De Robertis, A., Schell, C., and Jaffe, J. S. (2003). Acoustic observations of the swimming behavior of the euphausiid *Euphausia pacifica* Hansen. *ICES Journal of Marine Science*, 60:885–898.

Denman, K. and Platt, T. (1978). Time series analysis in marine ecosystems. In Shugart, H. H., editor, *Time Series and Ecological Processes*, pages 227–242. Society for Industrial and Applied Mathematics.

Denman, K. L. and Dower, J. F. (2001). Patch dynamics. In Steele, J. H., Turekian, K. K., and Thorpe, S. A., editors, *The Encyclopedia of Ocean Sciences*. Academic Press.

Denman, K. L. and Gargett, A. E. (1995). Biological-physical interactions in the upper ocean: The role of vertical and small scale transport processes. *Annual Review of Fluid Mechanics*, 27:225–255.

Dower, J. F., Miller, T. J., and Leggett, W. C. (1997). The role of microscale turbulence in the feeding ecology of larval fish. *Advances in Marine Biology*, 31:171–220.

Dower, J. F., Pepin, P., and Leggett, W. C. (1998). Enhanced gut fullness and an apparent shift in size selectivity by radiated shanny (*Ulvaria subbifurcata*) larvae in response to increased turbulence. *Canadian Journal of Fisheries and Aquatic Sciences*, 55:128–142.

Farmer, D. and Armi, L. (1999). Stratified flow over topography: the role of small-scale entrainment and mixing in flow establishment. *Proceedings of the Royal Society of London A*, 455:3221–3258.

Folt, C. L. and Burns, C. W. (1999). Biological drivers of zooplankton patchiness. *Trends in Ecology and Evolution*, 14(8):300–305.

François, R. E. and Garrison, G. R. (1982). Sound absorption based on ocean measurements: Part I: Pure water and magnesium sulfate contributions. *Journal of the Acoustical Society of the Americas*, 72(3):896–907.

Freeland, H. J. and Farmer, D. M. (1980). Circulation and energetics of a deep, strongly stratified inlet. *Canadian Journal of Fisheries and Aquatic Sciences*, 37:1398–1410.

Gallager, S. M., Davis, C. S., Epstein, A. W., Solow, A., and Beardsley, R. C. (1996). High-resolution observations of plankton spatial distributions correlated with hydrography in the Great South Channel, Georges Bank. *Deep-Sea Research II*, 43:1627–1663.

Gallager, S. M., Yamazaki, H., and Davis, C. S. (2004). Contribution of fine-scale vertical structure and swimming behavior to formation of plankton layers on Georges Bank. *Marine Ecology Progress Series*, 267:27–43.

Gargett, A. E. (1997). "Theories" and techniques for observing turbulence in the ocean euphotic zone. *Scientia Marina*, 61(Suppl. 1):25–45.

Greene, C. H., Widder, E. A., Youngbluth, M. J., Tamse, A., and Johnson, G. E. (1992). The migration behavior, fine structure, and bioluminescent activity of krill sound-scattering layers. *Limnology and Oceanography*, 37(3):650–658.

Hardy, A. C. and Bainbridge, R. (1954). Experimental observations on the vertical migrations of plankton animals. *Journal of the Marine Biological Association of the United Kingdom*, 33:409–448.

Haury, L. R., Kenyon, D. E., and Brooks, J. R. (1980). Experimental evaluation of the avoidance reaction of *Calanus finmarchicus*. *Journal of Plankton Research*, 2(3):187–202.

Haury, L. R. and Yamazaki, H. (1995). The dichotomy of scales in the perception and aggregation behavior of zooplankton. *Journal of Plankton Research*, 17(1):191–197.

Holliday, D. V. (1980). Use of acoustic frequency diversity for marine biological measurements. In Diemer, F. P., Vernberg, F. J., and Mirkes, D. Z., editors, *Advanced Concepts in Ocean Measurements for Marine Biology*, pages 423–460. University of South Carolina Press, South Carolina.

Holliday, D. V., Donaghay, P. L., Greenlaw, C. F., McGehee, D. E., McManus, M. M., Sullivan, J. M., and Miksis, J. L. (2003). Advances in defining fine- and micro-scale pattern in marine plankton. *Aquatic Living Resources*, 16:131–136.

Howlett, R. (1998). Sex and the single copepod. *Nature*, 394:423–424.

Jaffe, J. S., Ohman, M. D., and De Robertis, A. (1998). OASIS in the sea: measurement of the acoustic reflectivity of zooplankton with concurrent optical imaging. *Deep-Sea Research II*, 45:1239–1253.

Kathman, R. D., Austin, W. C., Saltman, J. C., and Fulton, J. D. (1986). *Identification Manual to the Mysidacea and Euphausiacea of the Northeast Pacific*, volume 93 of *Canadian Special Publication in Fisheries and Aquatic Sciences.*

Kiørboe, T., Saiz, E., and Viitasalo, M. (1996). Prey switching behavior in the planktonic copepod *Acartia tonsa*. *Marine Ecology Progress Series*, 143:65–75.

Lindström, M. and Fortelius, W. (2001). Swimming behaviour in *Monoporeia affinis* (Crustacea: Amphipoda)–dependence on temperature and population density. *Journal of Experimental Marine Biology and Ecology*, 256:73–83.

Lueck, R. G., Wolk, F., and Yamazaki, H. (2002). Oceanic velocity microstructure measurements in the 20th century. *Journal of Oceanography*, 58:153–174.

Mackas, D. L. and Boyd, C. M. (1979). Spectral analysis of zooplankton spatial heterogeneity. *Science*, 204:62–64.

Mackas, D. L., Denman, K. L., and Abbott, M. R. (1985). Plankton patchiness: biology in the physical vernacular. *Bulletin of Marine Science*, 37:652–674.

Mackas, D. L., Kieser, R., Saunders, M., Yelland, D. R., Brown, R. M., and Moore, D. F. (1997). Aggregation of euphausiids and pacific hake *Merluccius productus* along the outer continental shelf off vancouver island. *Canadian Journal of Fisheries and Aquatic Sciences*, 54:2080–2096.

Mackas, D. L., Sefton, H., Miller, C. B., and Raich, A. (1993). Vertical habitat-partitioning by large calanoid copepods in the oceanic subarctic Pacific during spring. *Progress in Oceanography*, 32:259–294.

Mackas, D. L., Trevorrow, M., Benfield, M., and Farmer, D. (2002). Zooplankton aggregation near sills. Office of Naval Research Report, FY02.

Macoun, P. (2003). *Buoyancy flux estimates for a tidal channel.* M.Sc. thesis, University of Victoria.

Macoun, P. and Lueck, R. G. (2004). Modelling the spatial response of the airfoil shear probe using different sized probes. *Journal of Atmospheric and Oceanic Technology*, 21(2):284–297.

McGehee, D. and Jaffe, J. S. (1996). Three-dimensional behavior of individual zooplankters: observations using the acoustical imaging system FishTV. *ICES Journal of Marine Science*, 53:363–369.

Medwin, H. and Clay, C. S. (1998). *Fundamentals of Acoustical Oceanography.* Academic Press.

Mudge, T. and Lueck, R. G. (1994). Digital signal processing to enhance oceanographic observations. *Journal of Atmospheric and Oceanic Technology*, 11:825–836.

Mutlu, E. (1996). Target strength of the common jellyfish (*Aurelia aurita*): a preliminary experimental study with a dual-beam acoustic system. *ICES Journal of Marine Science*, 53:309–311.

Nasmyth, P. W. (1970). *Oceanic turbulence.* Ph.D. thesis, University of British Columbia.

Osborn, T. R. and Crawford, W. R. (1980). An airfoil probe for measuring turbulence velocity fluctuation in water. In Dobson, L. H. F. W. and Davis, R., editors, *Air-Sea Interaction*, pages 369–386. Plenum, New York.

Pinel-Alloul, B. (1995). Spatial heterogeneity as a multiscale characteristic of zooplankton community. *Hydrobiologia*, 300/301:17–42.

Ritz, D. A. (2000). Is social aggregation in aquatic crustaceans a strategy to conserve energy? *Canadian Journal of Fisheries and Aquatic Sciences*, 57(Supp. 3):59–67.

Ross, T. (2003). *Sound scattering from oceanic turbulence.* Ph.D. thesis, University of Victoria.

Ross, T. and Lueck, R. (2003). Sound scattering from oceanic turbulence. *Geophysical Research Letters*, 30(6):1343.

Ross, T. and Lueck, R. (2004). Simultaneous acoustic observations of turbulence and zooplankton in the ocean. *Deep-Sea Research II*, in press.

Selivanovsky, D. A., Didenkulov, I. N., and Stunzhas, P. A. (1995). Acoustical investigation of phytoplankton. In *ICES International Symposium on Fisheries and Plankton Acoustics, Aberdeen (UK), 12-16 June 1995.*

Stanton, T. K. (1988). Sound scattering by cylinders of finite length. I. Fluid cylinders. *Journal of the Acoustical Society of America*, 83(1):55–63.

Stanton, T. K. (1989a). Simple approximate formulas for backscattering of sound by spherical and elongated objects. *Journal of the Acoustical Society of America*, 86(4):1499–1510.

Stanton, T. K. (1989b). Sound scattering by cylinders of finite length. III. Deformed cylinders. *Journal of the Acoustical Society of America*, 86(2):691–705.

Stanton, T. K. and Chu, D. (2000). Review and recommendations for the modelling of acoustic scattering by fluid-like elongated zooplankton: euphausiids and copepods. *ICES Journal of Marine Science*, 57:729–807.

Stanton, T. K., Chu, D., and Wiebe, P. H. (1996). Acoustic scattering characteristics of several zooplankton groups. *ICES Journal of Marine Science*, 53:289–295.

Stanton, T. K., Chu, D., and Wiebe, P. H. (1998). Sound scattering by several zooplankton groups. II. Scattering models. *Journal of the Acoustical Society of America*, 103:236–253.

Stanton, T. K., Chu, D., Wiebe, P. H., and Clay, C. S. (1993a). Average echoes from randomly oriented random-length finite cylinders: Zooplankton models. *Journal of the Acoustical Society of America*, 94(6):3463–3472.

Stanton, T. K., Clay, C. S., and Chu, D. (1993b). Ray representation of sound scattering by weakly scattering deformed fluid cylinders: Simple physics and application to zooplankton. *Journal of the Acoustical Society of America*, 94(6):3454–3462.

Stanton, T. K., Wiebe, P. H., Chu, D., Benfield, M. C., Canlon, L., Martin, L., and Eastwood, R. L. (1994). On acoustic estimates of zooplankton biomass. *ICES Journal of Marine Science*, 51:505–512.

Stone, D. P. (1977). *Copepod distributional ecology in a glacial run-off fjord.* Ph.D. thesis, University of British Columbia.

Strickler, J. R. (1998). Observing free-swimming copepods mating. *Philosophical Transactions of the Royal Society of London B*, 353:671–680.

Tiselius, P. (1992). Behavior of *Acartia tonsa* in patchy food environments. *Limnology and Oceanography*, 37(8):1640–1651.

Trevorrow, M. (2001). Zooplankton aggregations near a coastal sill: an examination of echo-sounder data from August and September 1995 in Knight Inlet, B.C. DREA Technical Memorandum 2001-119, Defence Research Establishment Atlantic, Dartmouth, NS. 35 pages.

Trevorrow, M. V. (2002). Zooplankton aggregations near sills. Office of Naval Research Report, FY02.

Vagle, S., Foote, K. G., Trevorrow, M. V., and Farmer, D. M. (1996). A technique for calibration of monostatic echosounder systems. *IEEE Journal of Oceanic Engineering*, 21(3):298–305.

Wiebe, P. H., Stanton, T. K., Benfield, M. C., Mountain, D. G., and Greene, C. H. (1997). High-frequency acoustic volume backscattering in the Georges Bank coastal region and its interpretation using scattering models. *IEEE Jouranl of Oceanic Engineering*, 22(3):445–464.

Yamada, Y., Ikeda, T., and Tsuda, A. (2002). Abundance, growth and life cycle of the mesopelagic amphipod *Primno abyssalis* (Hyperiidea: Phrosinidae) in the Oyashio region, western subarctic Pacific. *Marine Biology*, 141:333–341.

Yamazaki, H., Mackas, D. L., and Denman, K. L. (2002). Coupling small-scale physical processes with biology. In Robinson, A. R., McCarthy, J. J., and Rothschild, B. J., editors, *The Sea, Volume 12.* John Wiley & Sons Inc., New York.

Yamazaki, H. and Squires, K. D. (1996). Comparison of oceanic turbulence and copepod swimming. *Marine Ecology Progress Series*, 144:299–301.

Yen, J., Weissburg, M. J., and Doall, M. H. (1998). The fluid physics of signal perception by mate-tracking copepods. *Philosophical Transactions of the Royal Society of London Series B*, 353:787–804.

Appendix A

Zooplankton Taxa and Sizes

Table A.1 below lists the zooplankton taxa found in Knight Inlet in June, 2001, and the characteristic lengths (total length) for each. This list represents the groups into which zooplankton samples collected with the nets were sorted and then counted.

Taxon	*Genera/species or group (stage)*	*Length [mm]*
Amphipoda	*Cyphocaris challengeri*	10.5-13
		5.5-7.5
		3.5-4
	Primno abyssalis	10.1-11.4
		5.2-7
	Themisto pacifica	5.8-6.5
Brachyura	Pagurid (zoea)	8
Bryozoa	*Cyphonautes* (larvae)	0.3-0.5
Caridea	*Caridea mysis*	6
		7
		8
		9
		10
	Pasiophaea pacifica	46
Chaetognatha	*Eukrohnia hamata*	7.5
	Sagitta elegans	7.5
		15
Cirripedia	Cirriped (cyprid)	0.9

Taxon	*Genera/species or group (stage)*	*Length [mm]*
	Cirriped (nauplii)	0.7
Cladocera	*Evadne*	0.5-0.7
	Podon	0.3-0.6
Copepoda	*Acartia*	0.4-0.7
	Acartia hudsonica	0.8-1.1
	Acartia longiremis	0.9-1.3
	Aetideus divergens	1.5-1.9
	Calanus marshallae	2.8-3.3
	Calanus pacificus	2.1-2.6
	Corycaeaus anglicus	0.8-1.1
	Eucalanus	3.4-3.7
	Eucalanus bungii	4.9-6.8
	Euchaeta	3.8-4.2
	Euchaeta elongata	5.5-6.3
	Gaetanus minutus	2.9-3.2
	Heterorhabdus tanneri	3.1-4.2
	Metridia	7-1.2
	Metridia okhotensis	3.8-4.3
	Metridia pacifica	2-2.8
	Microcalanus pusillus	0.7-0.9
	Microcalanus pygmeus	0.7-0.9
	Oithona atlantica	1.1-1.4
	Pseudocalanus mimus	1.1-1.5
	Pseudocalanus minutus	1.4-1.9
	Pseudocalanus moultoni	1.2-1.6
	Scolecithricella minor	1.2-1.4
	Tortanus discaudatus	1.4-2
	Copepod (nauplii)	0.2-0.4
Ctenophora	*Pleurobrachia bachei*	13
Euphausiacea	*Euphausia pacifica*, female	11
		12
		13
		22

Taxon	*Genera/species or group (stage)*	*Length [mm]*
		23
		24
		25
	Euphausia pacifica, male	20
		21
		22
	Euphausia pacifica (juvenile)	5
		6
		7
		8
		9
		10
	Thysanoessa longipes	8
	Euphausiid (eggs)	0.35
	Euphausiid (nauplii)	0.4
	Euphausiid (protozoea)	0.8-1.5
	Euphausiid (zoea)	1.8-3
Foraminifera	*Globeringa*	0.3
Larvacea	*Fritellaria borealis*	3.5-3.7
	Oikopleura dioica	3.5-4.6
	Oikopleura labradoriensis	7.4-8.3
Medusa	*Aegina citrea*	5.2-6.1
	Aglantha digitale	5.8-7
	Melicertum octocostatum	10.2
	Obelia	0.3
	Phialidium gregarium	10.3
	Proboscidactyla flavicirrata	5.1-5.5
	Sarsia	6.5
Mollusca	*Limacina helicina*	0.5-1.2
Mysidacea	*Alienocanthomysis macropsis*	6
	Neomysis rayi	18
Ostracoda	*Alata minor*	1.6-2

Taxon	*Genera/species or group (stage)*	*Length [mm]*
	Disconchoecia elegans	1.2-2.2
Pisces	*Clupea pallsai*	19
	Leuroglossus schmidti	8
	Liparid	8
	Mallotus villosus	15
		17
		22
Polychaeta	Polynoid (larvae)	1.9-2.4
	Spionid (larvae)	1.4-1.9
	Syllid (epitoke)	8.3
	Tomopteris pacifica	7
		14
		25
		52
	Tomopteris septrionalis	10
		14
		15
		16
Siphonophora	*Dimophyes arctica*	3.8-4.4
		6.3-8.1
	Nanomia bijuga	5-5.3

Table A.1: Zooplankton taxa observed in Knight Inlet in June, 2001, and characteristic length ranges. Where more than one length is listed for a single species, the members of that species were sorted into the size classes shown. All lengths are total lengths.